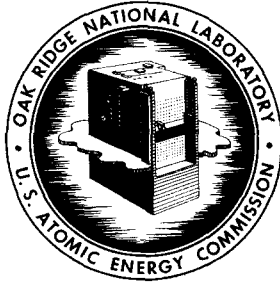




3 4456 0513474 3



OAK RIDGE NATIONAL LABORATORY

operated by

**UNION CARBIDE CORPORATION
NUCLEAR DIVISION**



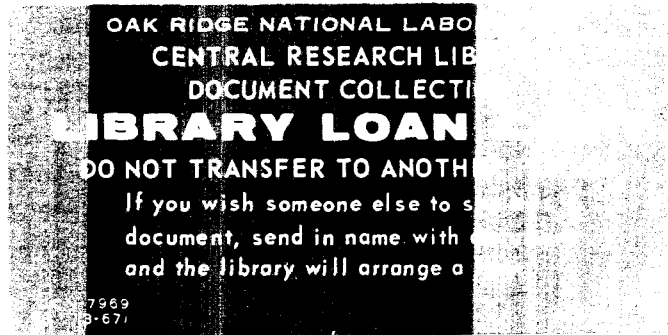
for the
U.S. ATOMIC ENERGY COMMISSION

ORNL - TM - 2030

2

**LOW ENERGY ELECTRON STUDIES IN ALUMINUM
(Thesis)**

S. J. Nalley, M. Y. Nakai, F.W. Garber
R. H. Ritchie, J. A. Harter, and R. D. Birkhoff



Submitted by S. J. Nalley as a dissertation to the Graduate School of the University of Tennessee in partial fulfillment of the requirements for the degree of Master of Science in Physics.

LEGAL NOTICE

This report was prepared as an account of Government sponsored work. Neither the United States, nor the Commission, nor any person acting on behalf of the Commission:

- A. Makes any warranty or representation, expressed or implied, with respect to the accuracy, completeness, or usefulness of the information contained in this report, or that the use of any information, apparatus, method, or process disclosed in this report may not infringe privately owned rights; or
- B. Assumes any liabilities with respect to the use of, or for damages resulting from the use of any information, apparatus, method, or process disclosed in this report.

As used in the above, "person acting on behalf of the Commission" includes any employee or contractor of the Commission, or employee of such contractor, to the extent that such employee or contractor of the Commission, or employee of such contractor prepares, disseminates, or provides access to, any information pursuant to his employment or contract with the Commission, or his employment with such contractor.

Contract No. W-7405-eng-26

HEALTH PHYSICS DIVISION

LOW ENERGY ELECTRON STUDIES IN ALUMINUM

S. J. Nalley, M. Y. Nakai, F. W. Garber

R. H. Ritchie, J. A. Harter, and R. D. Birkhoff

Submitted by S. J. Nalley as a dissertation to the
Graduate School of The University of Tennessee in
partial fulfillment of the requirements
for the degree of
Master of Science in Physics

JANUARY 1968

OAK RIDGE NATIONAL LABORATORY
Oak Ridge, Tennessee
operated by
UNION CARBIDE CORPORATION
for the
U. S. ATOMIC ENERGY COMMISSION

LOCKHEED MARTIN ENERGY RESEARCH LIBRARIES



3 4456 0513474 3

ACKNOWLEDGMENTS

The authors would like to express their gratitude to A. G. Kenerly for his assistance in electronic problems and in maintaining the equipment, and to Beverly Varnadore for typing the manuscript.

One of the authors (SJN) would also like to express his appreciation to the Health, Education and Welfare Department for their support of his research through its Radiological Health Physics Fellowship which is administered by the University of Tennessee.

TABLE OF CONTENTS

CHAPTER	PAGE
I. INTRODUCTION	1
II. GENERAL CONSIDERATIONS	2
Previous Work on Low Energy Electron Transmission in Solids	2
Types of Interactions of Low Energy Electrons with Solids . .	3
Mean Free Paths of Electrons Near the Fermi Energy . . .	3
Surface Plasmon Cross Section	4
Volume Plasmon Interactions	7
Inner Shell Interactions	8
III. EXPERIMENTAL	15
Outline of the Experimental Method	15
Equipment	17
Vacuum System	17
Electron Gun	20
Current Measuring System	25
Secondary Electron Suppressor Assembly	29
Procedure	30
Target Preparation	30
Experimental Procedure	38
IV. RESULTS AND DISCUSSION	42
V. CONCLUSIONS	53
BIBLIOGRAPHY	55

LIST OF FIGURES

FIGURE	PAGE
1. Theoretical Stopping Power of Aluminum due to Electron-Electron Interactions and Electron-Volume Plasmon Interactions for Low Energy Electrons and the Sum of These	9
2. Theoretical and Experimental Stopping Power for L-Shell Interactions	12
3. Theoretical Probability of L-Shell Interactions for a 250 Å Thick Aluminum Target.	13
4. Complete Transmission Length as a Function of Energy and Comparison with Kanter and Sternglass' Range-Energy Measurements	14
5. Cross Section of Target.	16
6. Photograph of Apparatus	18
7. Vacuum System Cross Section	19
8. Cross Section of Evaporation Chamber, Electron Gun, Rotation Mechanism and Mechanical Shutter	21
9. Electron Gun Circuit Diagram	22
10. Photograph of Electron Gun	23
11. Schematic Diagram of Current Measuring System	26
12. Operational Diagram for Ratiometer	28
13. Top View of Sandwich	33
14. Schematic Diagram of Anodic Oxidation Apparatus.	34
15. Oxide Thickness Versus Applied Voltage	35

FIGURE	PAGE
16. Photograph of Completed Target	37
17. Circuit Diagram of Rotating Switch for Electronic Shutter	40
18. Top Current as a Function of Incident Electron Energy for a 180 Å Thick Aluminum Foil with Various Bias Voltages	43
19. Attenuation Lengths in Aluminum for Electrons of <60 e.V. Energy	44
20. Top Current as a Function of Incident Electron Energy for a 155 Å Thick Aluminum Foil at Incident Angles of θ and 45 Degrees	46
21. Top Current as a Function of Incident Electron Energy for a 200 Å Thick Aluminum Foil at Incident Angles of 0, 45, and 60 Degrees	47
22. Top Current as a Function of Incident Electron Energy for a 240 Å Thick Aluminum Foil at Incident Angles of 0 and 45 Degrees	48
23. Top Current as a Function of Incident Electron Energy for a 240 Å Thick Aluminum Foil at Incident Angles of 30 and 60 Degrees	49
24. Top Current as a Function of Incident Electron Energy for a 280 Å Thick Aluminum Foil at Incident Angles of 0 and 45 Degrees	50
25. Top Current as a Function of Incident Electron Energy for a 280 Å Thick Aluminum Foil at Incident Angles of 30 and 60 Degrees	51

CHAPTER I

INTRODUCTION

The volume plasmon theory, proposed by Bohm and Pines (1951) and the surface plasmon theory proposed by Ritchie (1957) predict the excitation of surface plasmons and volume plasmons by electrons which penetrate solids. These excitations in thin metallic films have been the subject of study by Garber (1965) and Pray (1966). It was the purpose of this investigation to examine the dependence upon the angle of incidence of the primary beam to the surface plasma excitation utilizing an ultrahigh vacuum system to obtain cleaner surfaces. Also of interest was the effect upon these excitations of various amounts of secondary electron suppression.

A nearly monoenergetic beam of electrons was incident upon a thin ($< 300 \text{ \AA}$) aluminum film deposited under ultrahigh vacuum conditions ($\sim 10^{-9}$ torr) as the top layer of an Al-Al₂O₃-Al diode. The currents from the top and bottom layers were then measured as a function of electron energy. The top current was expressed as a fraction of the total current and plotted versus the primary energy. The effect of various amounts of suppression voltage on the currents has been investigated under normal vacuum conditions (10^{-6} torr). Substantial differences were noted which indicated that except at the lowest electron energies ($< 60 \text{ e.V.}$) and the highest ($> 500 \text{ e.V.}$), no electron transport took place across the top layer which could lead to traversal of the Al₂O₃ dielectric.

CHAPTER II

GENERAL CONSIDERATIONS

In this chapter consideration is given to previous work on low energy electron studies in thin solid films. Attention is given to three types of interactions: surface plasma excitation, volume plasma excitation, and inner shell interactions.

I. PREVIOUS WORK ON LOW ENERGY ELECTRON TRANSMISSION IN SOLIDS

For several years interest has been centered on the characteristic energy losses of electrons in solids. Experimenters sought to determine electronic energy levels in solids using an incident electron beam of high energy. Several review articles give adequate discussion of previous work [L. Marton et al. (1955), L. Marton (1956), R. H. Ritchie (1957), Klemperer and Shepherd (1963), R. D. Birkhoff (1964), G. Höhler (1965), R. H. Ritchie, M. Y. Nakai, and R. D. Birkhoff (1967)].

The theory which best seems to explain the characteristic energy losses is the collective excitation or plasmon model originated by Bohm and Pines (1951). This model has been studied by investigators both theoretically and experimentally. Some losses below the plasmon energies have been interpreted by Ritchie (1957) as surface plasmon excitations.

II. TYPES OF INTERACTIONS OF LOW ENERGY ELECTRONS WITH ALUMINUM

Mean Free Paths of Electrons Near the Fermi Energy

First we consider electrons with energies between the Fermi level and the plasmon threshold. An electron with energy one volt or less above the Fermi level will have a very long mean free path. This is easily understood, because after collision, both the primary and secondary electrons must have energies above the Fermi level. Thus, as an energetic electron slows down closer and closer to the Fermi energy, the number of electrons with which it may interact is effectively reduced. Attenuation lengths have been calculated to be 520 Å [see Ritchie et al. (1967)] for silver for electrons with energies near the Fermi level. The attenuation is due to electron-phonon as well as electron-electron scattering. We concern ourselves with attenuation lengths because the several processes involved prevent a precise determination of the mean free path for a particular process. The attenuation length is more easily interpreted experimentally as the distance in which a beam of electrons is reduced to $\frac{1}{e}$ of its original intensity.

For comparison with other metals we cite the results of several researchers. Quinn (1962) has calculated the electron-electron mean free path to be 560 Å in silver, a slightly higher figure than the 440 Å obtained through the experiments of Crowell, Spitzer, Howarth, and LaBate (1962). For gold, Crowell et al. (1962) obtained a 740 Å attenuation length. In so

doing they assumed that the optical absorption of gold on silver was the same as that for gold on glass. This assumption was found unreasonable by Soshea and Lucas (1965) who, using correct optical data, obtained an electron attenuation length of 350 Å.

A method avoiding the problems inherent in the optical method for determining attenuation lengths and mean free paths has been given by Crowell and Sze (1965). They injected electrons into a thin metallic film, supported by a Ge or Si substrate, through a Si point contact. This method has produced attenuation lengths in gold of between 229 and 372 Å, values in reasonable agreement with that of Soshea and Lucas.

A tabular listing of the data of several investigators for Ag, Pd, Cu, and Au is given in Table I.

Surface Plasmon Cross Section

Above 10 e.V. in aluminum, surface plasmon excitation by incident electrons is thought to occur with high probability. The equation relating surface plasma frequency to volume plasma frequency for an ideal free electron metal has been given by Ritchie as

$$\hbar\omega_s = \frac{1}{\sqrt{1+\epsilon_0}} \hbar\omega_v, \quad (1)$$

where ω_v is the volume plasma frequency; ω_s is the surface plasma frequency, \hbar is Planck's constant and ϵ_0 is the dielectric constant of the medium bounding the investigated surface.

TABLE I

ATTENUATION LENGTHS AND MEAN FREE PATHS FOR ELECTRONS

Element	Attenuation Lengths (Å)	Electron-Electron Mean Free Path (Å)	Electron-Phonon Mean Free Path (Å)	Investigator	
Ag		560*		Quinn (1962)	
			950*	Quinn (1963)	
		520*		Ritchie <i>et al.</i> (1965)	
		440		Crowell <i>et al.</i> (1962)	
			570*	Mott and Jones (1958)	
Pd	170			Crowell <i>et al.</i> (1962)	
Cu	50-200			Crowell <i>et al.</i> (1962)	
			420*	Mott and Jones (1958)	
				720*	Quinn (1962)
				1580*	Quinn (1963)
			580*		Ritchie <i>et al.</i> (1965)
Au	740	415*		Crowell <i>et al.</i> (1962)	
	350			Soshea and Lucas (1965)	
	229†			Crowell and Sze (1965)	
	357‡			Crowell and Sze (1965)	
			523*	Ritchie <i>et al.</i> (1967)	

*Theoretical value

†Observed at 298°K

‡Observed at 105°K

In the case that the crystal is bounded by vacuum, ϵ_0 is unity. The surface plasma frequency then becomes

$$\hbar\omega_s = \frac{1}{\sqrt{2}} \hbar\omega_v \quad . \quad (2)$$

For normal incidence, the probability for a surface plasma excitation by a relatively energetic incident electron is

$$P(E) = \frac{\pi}{1 + \epsilon_0} \left[\frac{Ry}{E} \right]^{\frac{1}{2}} \quad , \quad (3)$$

where $E \gg E_s$. Here E_s is the energy of the surface plasmon; E is the energy above the vacuum level of the incident electron; and Ry is Rydberg's constant, 13.60 e.V.

For an incidence angle of θ , primarily for θ near $\pi/2$

$$P(E) = \frac{4}{1 + \epsilon_0} \left[\frac{Ry}{E} \right]^{\frac{1}{2}} \frac{1}{\cos \theta} \quad . \quad (4)$$

For intermediate angles

$$P(E) = \frac{2}{\pi(1 + \epsilon_0)} \left[\frac{Ry}{E} \right]^{\frac{1}{2}} \int_0^x \frac{x dx}{(1+x)^2} \int_0^{2\pi} \left[\frac{1+x^2}{\cos^2 \theta} - (x \tan \theta \cos \Psi + 1)^2 \right]^{\frac{1}{2}} d\Psi \quad . \quad (5)$$

An inspection of equations (3) and (5) shows that $P(E)$ increases with θ .

While at high energies the Born approximation may be used to calculate the inverse mean free path, it may only be relied upon at lower energies ($E \simeq E_s$) to produce values of the correct order of magnitude. Still these equations give some indication of the angular dependence of the probability at low energies above the surface plasmon threshold.

The oxidation of the surface affects the energy of a surface plasmon. According to equation (1) when one finds an oxide layer on aluminum or magnesium, with a dielectric constant greater than one, the surface plasma frequency is lowered.

It has been shown [Stern and Ferrell (1960)] that a layer of dielectric constant ϵ and thickness of 20 Å is sufficient to force the use of equation (1) instead of (2). Consideration of these facts demonstrates the importance of performing experiments under ultrahigh vacuum conditions. If the ultrahigh vacuum system sufficiently decreases the oxidation rate, it is possible to neglect the dielectric constant of the surface oxide layer.

Volume Plasmon Interactions

In the energy region between 15 e.V. and 100 e.V., volume plasma excitation may occur.

Ritchie (1959) and Quinn (1962) derived results which make it possible to calculate the stopping power of aluminum for electrons of primary energy below the L_{23} shell threshold, 72 e.V. As mentioned above there are two dominant interactions in this energy region, electron-electron and volume plasma excitations. It is only in an energy region one to three times the Fermi energy that it is possible to write a simple expression for the stopping power due to electron-electron interactions:

$$-\left(\frac{dE}{dx}\right)_{ee} = \frac{0.073}{E} (E - 1)^3 . \quad (6)$$

In this relation the stopping power is in Fermi energies per angstrom where

E is the energy of the incident electrons in Fermi units. It is clear that electrons of a few tens of volts energy will slow to near the Fermi energy within a few angstroms.

It is possible to calculate $\frac{dE}{dx}$ from mean free paths. Quinn calculated the mean free path of a low energy electron for volume plasmon excitation. Birkhoff (1964) has shown this relation to be expressible as

$$\lambda = \frac{137 \beta^2 c}{\omega_p \ln \left[\frac{\sqrt{E_F + E_p} - \sqrt{E_F}}{\sqrt{E} - \sqrt{E - E_p}} \right]}, \quad (7)$$

where ω_p is the volume plasma frequency, E_p is the plasma energy, β is the ratio of electron velocity to the velocity of light, c , E_F is the Fermi energy and E is the energy of the incident electron in electron volts. Dividing the plasma energy of aluminum by this mean free path, one obtains the stopping power of aluminum for plasmon excitation;

$$\left(\frac{dE}{dx} \right)_{vp} = \frac{\hbar \omega_p^2 \ln \left[\frac{\sqrt{E_F + E_p} - \sqrt{E_F}}{\sqrt{E} - \sqrt{E - E_p}} \right]}{137 \beta^2 c} \quad (8)$$

Figure 1 gives the curves for the stopping powers of electron-electron and volume plasma interactions and the sum of the two.

Inner Shell Interactions

In the energy range from about 100 e.V. to the limit of this investigation, it is possible to have an interaction of the bombarding electron with

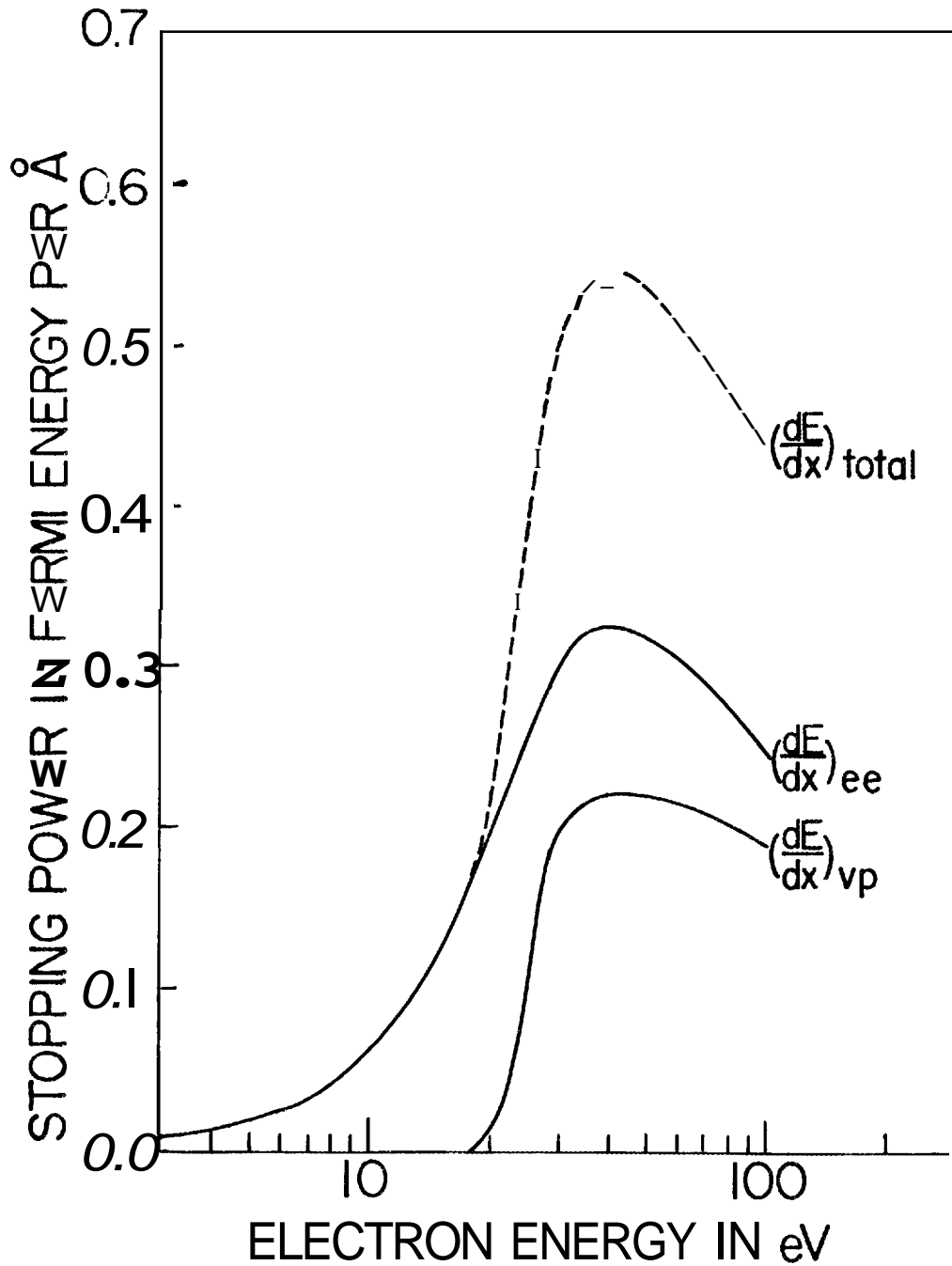


Figure 1. Theoretical Stopping Power of Aluminum due to Electron-Electron Interactions and Electron-Volume Plasmon Interactions for Low Energy Electrons and the Sum of These

the inner shell electrons of the target atom. The threshold for the L_2 -shell ionization is 72 e.V. and for the L_1 -shell 117 e.V.

One may use either the Born approximation or the Gryzinski (1965) classical approximation to calculate the electron-L-shell interaction cross section. Ritchie (1967) used the prescription of Walske (1956) to correct the Born approximation for K- and outer-shell screening.

The stopping power $-\left(\frac{dE}{dx}\right)$ of a given L-shell for electrons with energy $\eta Z_{\text{eff}}^2 \text{ Ry}$ is for $\eta = \frac{mv^2}{2} / Z_{\text{eff}}^2 \text{ Ry}$

$$-\frac{dE}{dx} = \frac{8\pi a_0^2 N}{z_{\text{eff}}^4 \eta} \int_{\theta/4}^{\eta} W dW \int_{\eta[1 - \sqrt{1 - \frac{W}{\eta}}]^2}^{\eta[1 + \sqrt{1 - \frac{W}{\eta}}]^2} g_1(Q, W) dQ, \quad (9)$$

where $k^2 = W - \frac{1}{4}$ and

$$g_1(Q, k) = \left\{ \frac{[Q^3 - (\frac{5}{3}k^2 + \frac{11}{12})Q^2 + (\frac{1}{3}k^4 + \frac{3}{2}k^2 + \frac{64}{48})Q + (\frac{1}{3}k^6 + \frac{3}{4} + \frac{23}{48}k^2 + \frac{5}{64})]}{Q[(Q - k^2 + \frac{1}{4})^2 + k^2]} \right\} \quad (10)$$

$$\times \exp \left\{ \frac{-2}{k} \tan^{-1} \left(\frac{2k}{Q - k^2 + \frac{1}{4}} \right) \right\} \left[\frac{2^4}{1 - e^{-2\pi r/k}} \right]$$

The quantity $(1 - e^{-2\pi r/k})$ is unity if k^2 becomes negative. W is the energy lost by the incident electron, and $Q = (\text{change in momentum of incident particle}) / (2M Z_{\text{eff}}^2 \text{ Ry})^{\frac{1}{2}}$. All energies are measured in units of $Z_{\text{eff}}^2 \text{ Ry}$. $Z_{\text{eff}} = (Z - 4.15)$. All L-shell electrons are assumed to have equal binding energies. θ is the ratio of the actual L-shell ionization energy to the

"effective" ionization energy $\frac{1}{4}Z_{\text{eff}}^2 \text{ Ry}$. N is the atomic density [Ritchie et al. (1967)]. Figure 2 gives a comparison of theoretical and experimental values for the L-shell stopping power.

An estimate of the probability of L-shell ionization in the energy region employed here may be made as follows. If P_o is the probability of reaching depth x without an L-shell interaction and dx/λ the probability of an interaction in the distance x to $x+dx$, then the probability for no interaction decreases according to

$$-dP_o = P_o \frac{dx}{\lambda(E)} \quad (11)$$

Using the relation $dx = dE/(dE/dx)$ and integrating we get

$$P_o = \exp \left[- \int_{E_2}^{E_1} \frac{dE}{\lambda(E) \frac{dE}{dx}(E)} \right] , \quad (12)$$

where E_1 is the initial electron energy, E_2 the energy with which the primary electron exits the top layer, $\lambda(E)$ the L-shell mean free path, and $\frac{dE}{dx}(E)$ the stopping power of the conduction electrons. A graph of $(1 - P_o)$, from Eq. 12 using values of $\lambda(E)$ and $\frac{dE}{dx}(E)$ from Ritchie et al. (1967) is given in Figure 3. Thus we see that the probability for an L-shell interaction is quite high in foils a few hundred angstroms in thickness.

As the primary energy increases past the maximum in the L-shell cross section, the range of the primary electron increases. These ranges have been calculated from experimental data by Kanter and Sternglass (1962) and Garber (1965). Their results are summarized in Figure 4.

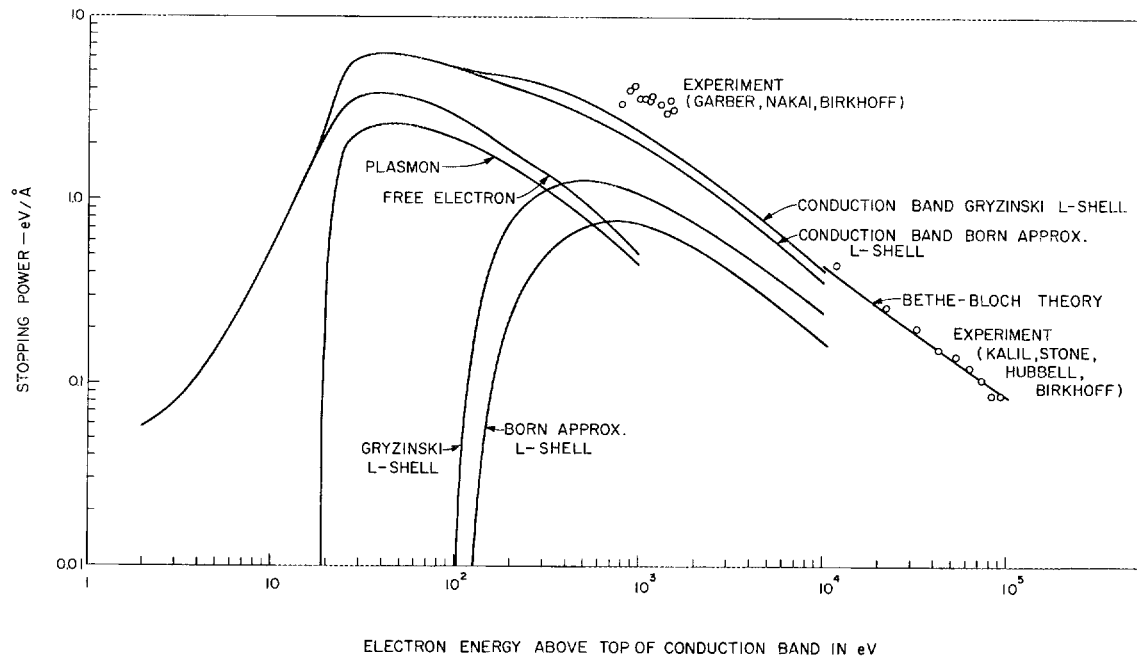


Figure 2. Theoretical and Experimental Stopping Power for L-Shell Interactions

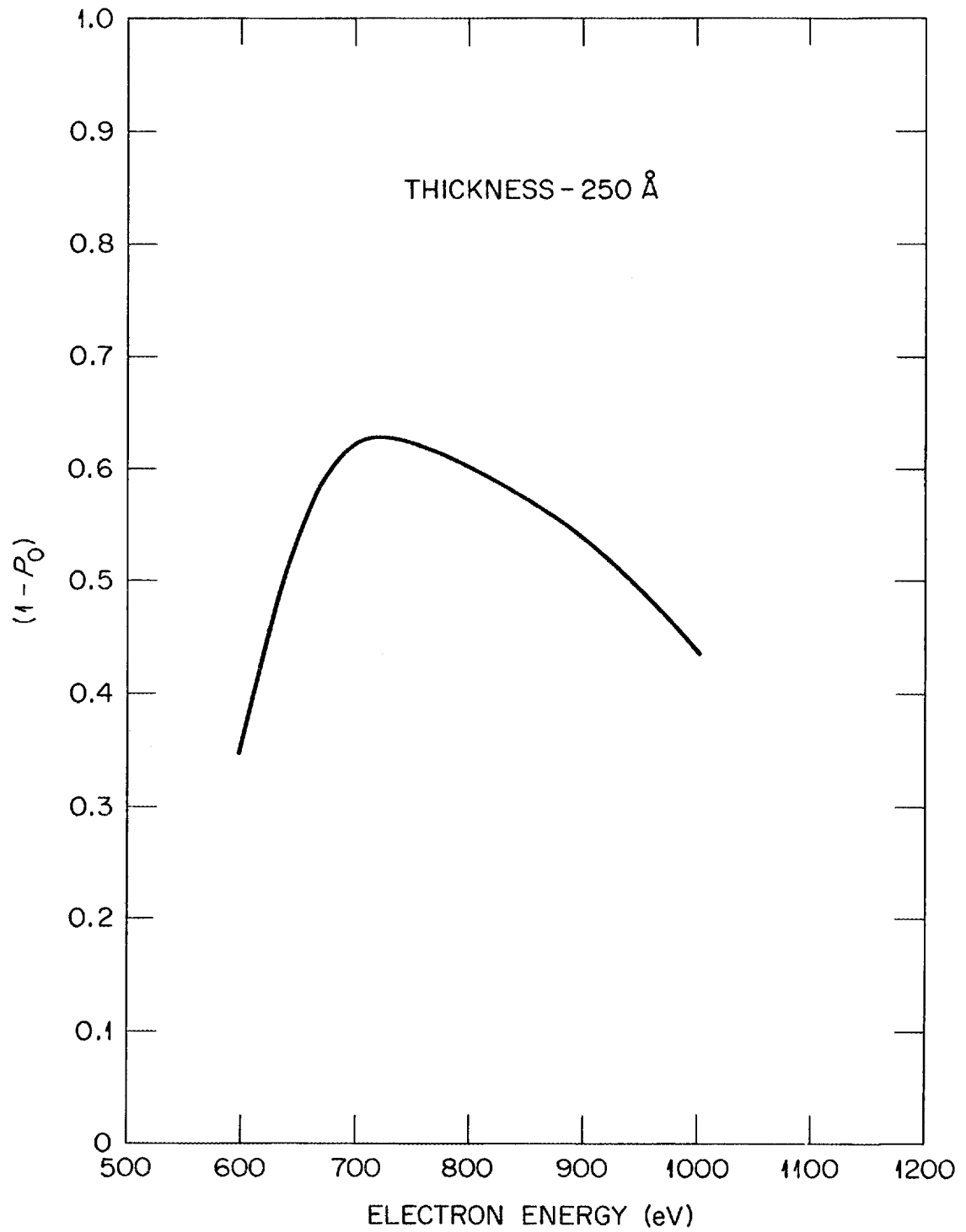


Figure 3. Theoretical Probability of L-Shell Interactions for a 250 Å Thick Aluminum Target

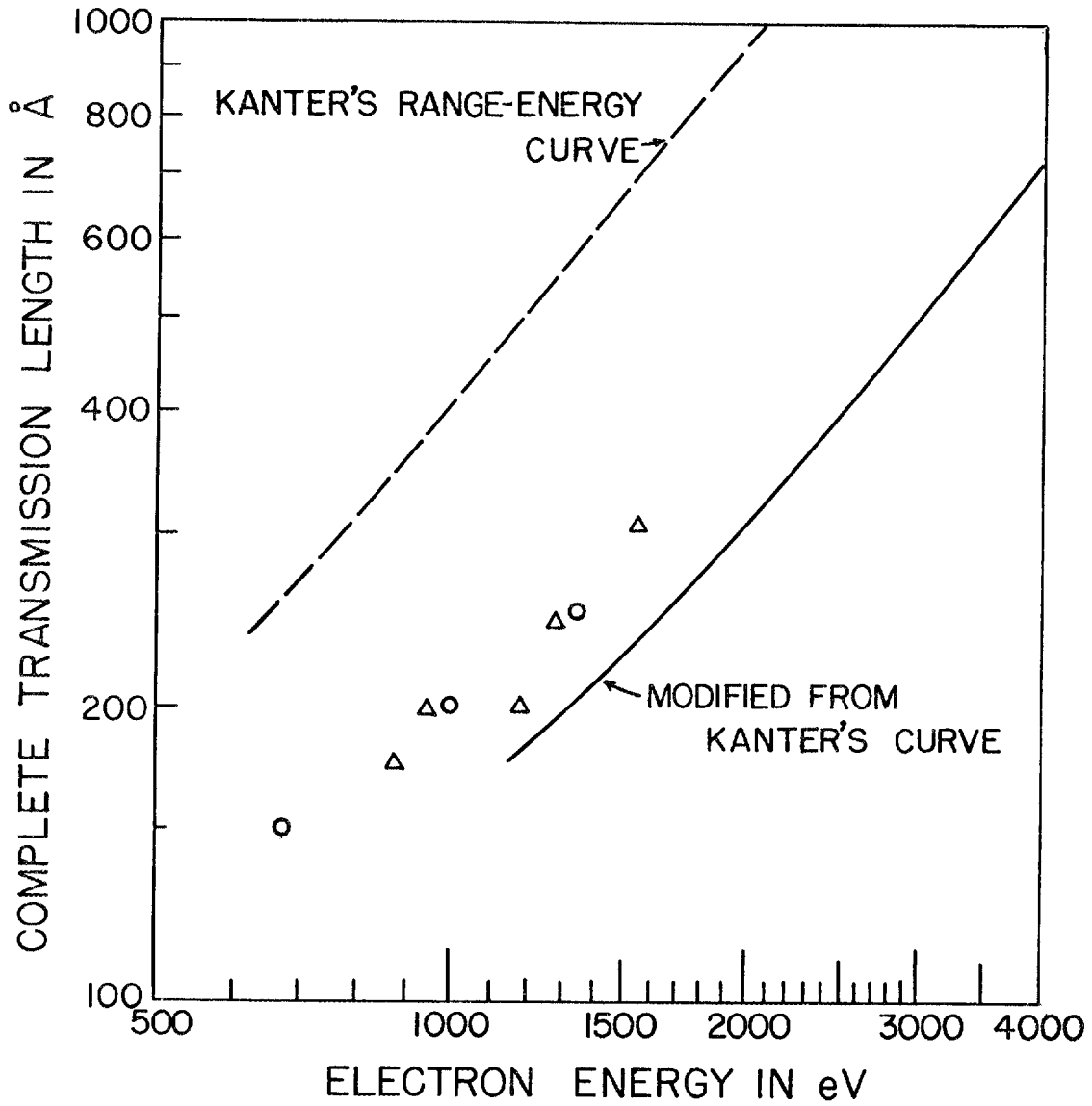


Figure 4. Complete Transmission Length as a Function of Energy and Comparison with Kanter and Sternglass' Range-Energy Measurements

CHAPTER III

EXPERIMENTAL

I. OUTLINE OF THE EXPERIMENTAL METHOD

In this experiment a beam of electrons was directed at a thin non-self-supporting film to determine the number of electrons, i. e., the fraction of current, that was stopped in the film due to absorption and scattering. Since these films of aluminum were of the order of 150 to 300 Å thick, it was necessary that there be a supporting substrate. As in previous work, we decided to use the aluminum-insulator-aluminum sandwich. The bottom layer was aluminum of high purity and of sufficient thickness to stop all electrons leaving the top layer. The insulator was aluminum oxide formed on the bottom layer of aluminum through an anodizing process. The top layer was then evaporated in the ultrahigh vacuum system to the desired thickness. A beam of electrons from an electron gun was incident upon the top layer either normally or at any desired angle. The currents to the film and conducting substrate were then measured as a function of energy. A cross-sectional view of this target is presented in Figure 5.

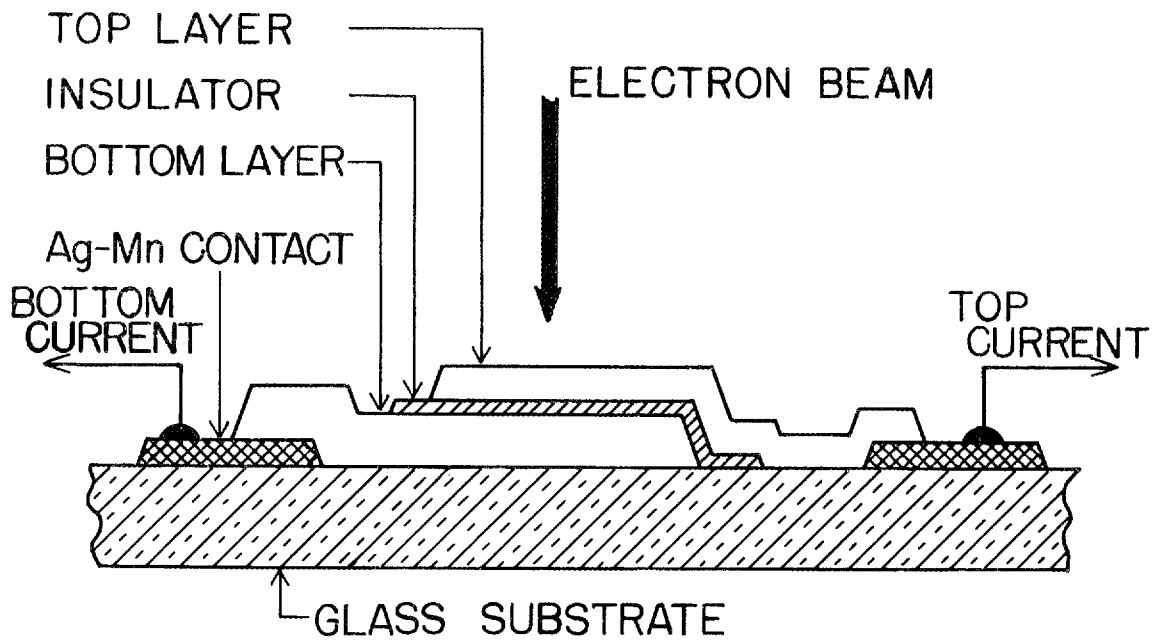


Figure 5. Cross Section of Target

II. EQUIPMENT

The vacuum system, the electron gun, and the current measuring system were the three major components involved in this work. A photograph of the apparatus is given in Figure 6.

Vacuum System

The vacuum system is shown in Figure 7. A National Research Corporation 6-inch, oil diffusion pump using Dow-Corning 705 fluid backed by a Welch Duo-Seal mechanical forepump constituted the pumping system. Oil back-streaming was reduced by incorporation of a Granville Phillips Company series 251 6-inch cryosorb liquid nitrogen cold trap. Mixing of forepump and diffusion pump oils is reduced by the incorporation of a molecular sieve in the vacuum line between the two pumps. Pressures before operation were normally 2×10^{-9} torr. These pressures were measured by an NRC Equipment Corporation Type 563-K ionization gauge, read by an NRC thermocouple and UHV ionization gauge control, model 763. The evaporation chamber was a 12-inch electropolished stainless steel pipe with a lower 10-inch flange to connect to the cold trap. All O-rings were diamond-shaped copper O-rings except the one between the system cover and a 16-inch upper flange which was of aluminum wire. The cover, made of 1-inch-thick stainless steel, was attached to the upper flange by means of twelve 5/8-inch stainless steel bolts and nuts. These were tightened to 175 foot-pounds of torque to properly seal the aluminum O-ring.

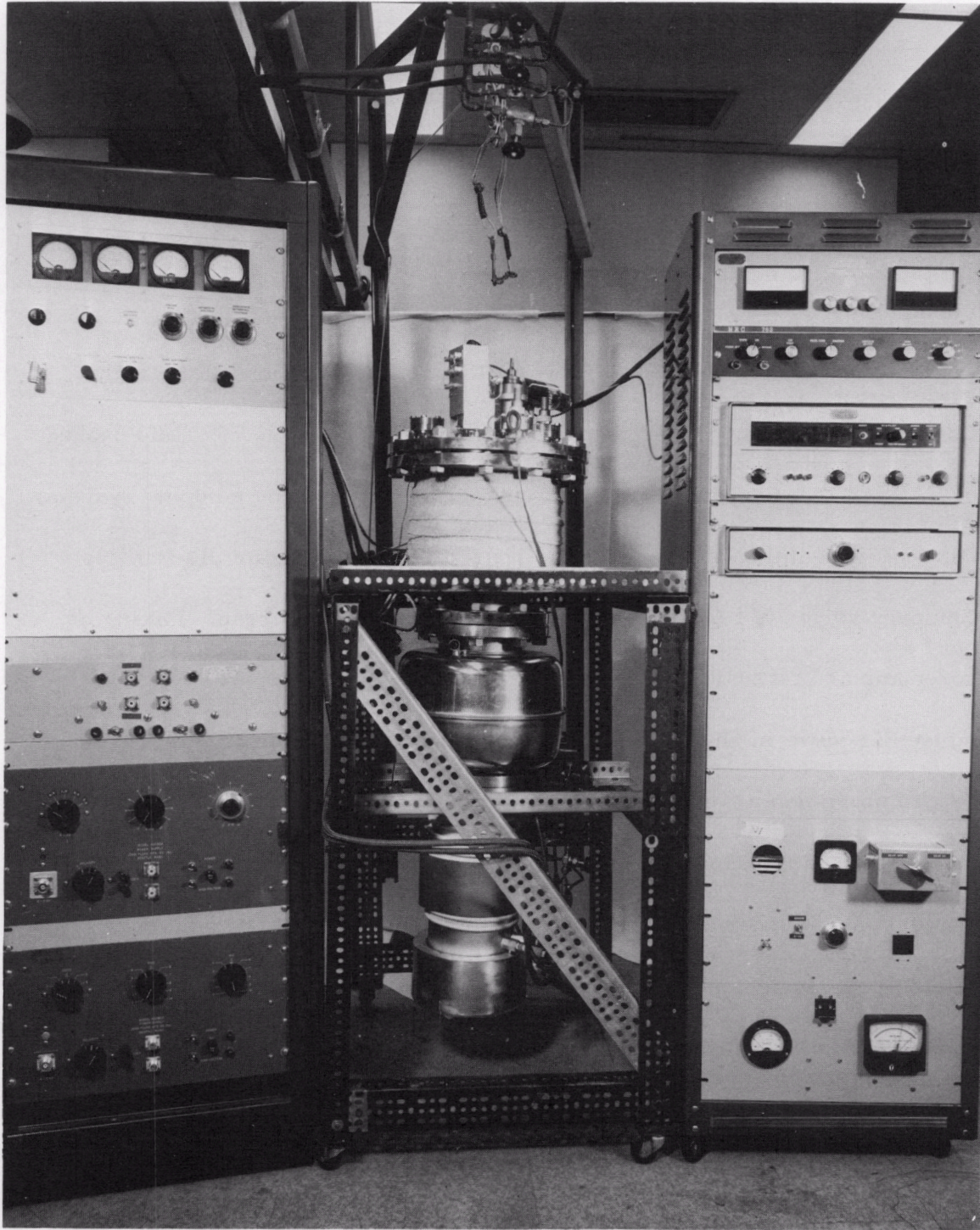


Figure 6. Photograph of Apparatus

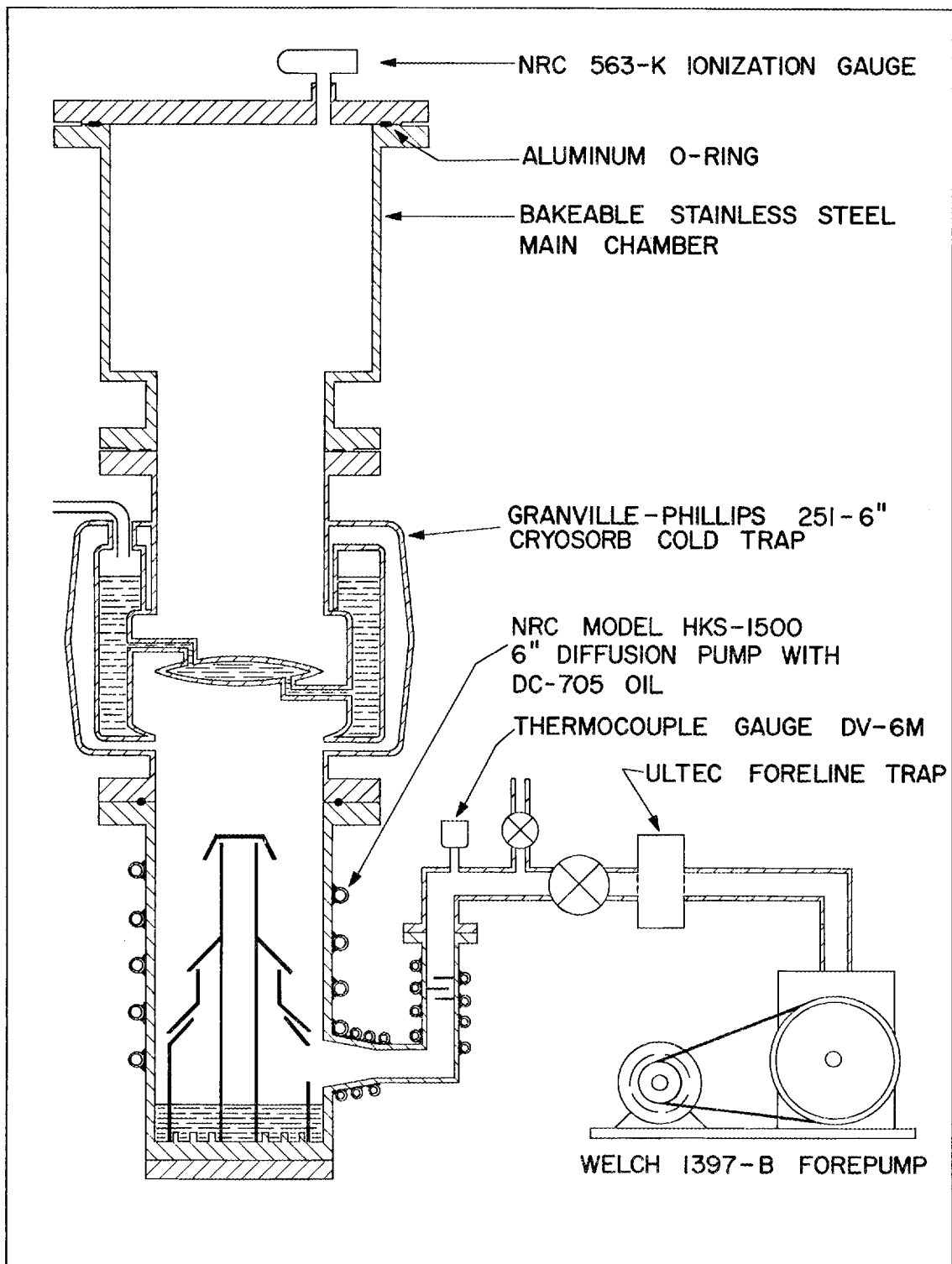


Figure 7. Vacuum System Cross Section

This cover served as a mounting platform for all internal equipment except the film thickness monitoring crystal which was mounted upon a dividing plate which separated the evaporation source and the film substrate. Eight 1 1/4-inch inside diameter feedthroughs equipped with non-rotatable conflat flanges. Varian number 954-5069, were located at all access ports. The flanges were equipped with standard flat copper O-rings and were capped by the proper feedthroughs. There were two eight-wire current feedthroughs, Varian model 954-5014, with conflat flanges which provided electrical contact with the gun, sandwich, and film thickness monitor. Two threaded copper bar feedthroughs supplied current to the evaporation boat. Two linear motion feedthroughs permitted movement of the mechanical shutter between substrate and evaporation source, and rotation of the target. This arrangement is seen in Figure 8. A Speedivac film thickness monitor, Model 1, was used to determine film thickness.

Electron Gun

Previous research had made use of a gun whose lowest energy range was about 6 e.V. To go below this energy, it was necessary to alter the design of the electron gun. The gun used was modified from a design used by Compton *et al.* (1966). The lowest energy was on the order of 1.0 e.V. with an energy spread, which varied from 10% at the lowest energy to 3% at 100 e.V. and above. The gun, which is shown in Figures 9 and 10, was composed of a stack of five stainless-steel plates numbered from 1-5. The filament was positioned near the aperture in plate one. A narrow

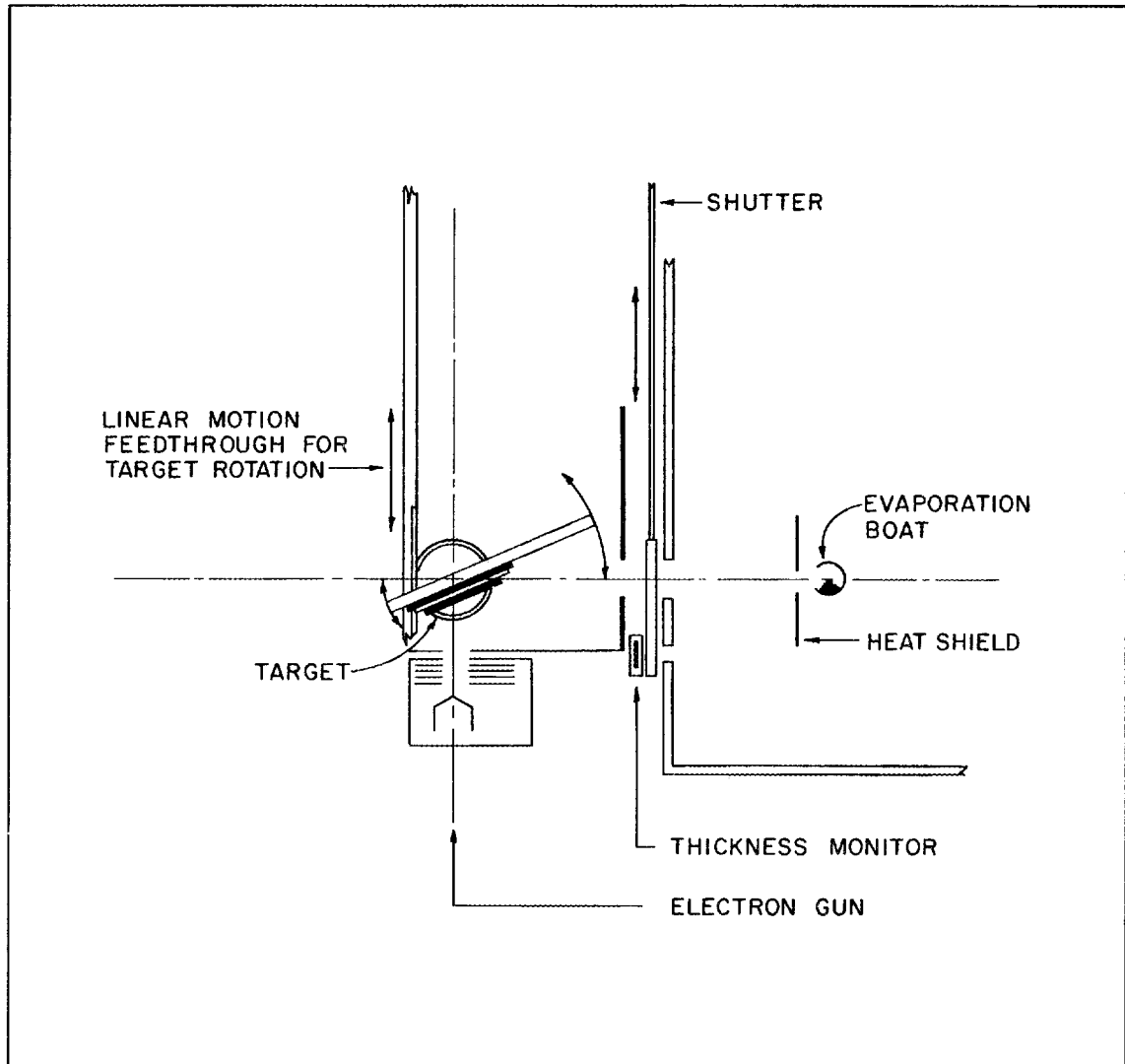


Figure 8. Cross Section of Evaporation Chamber, Electron Gun, Rotation Mechanism and Mechanical Shutter

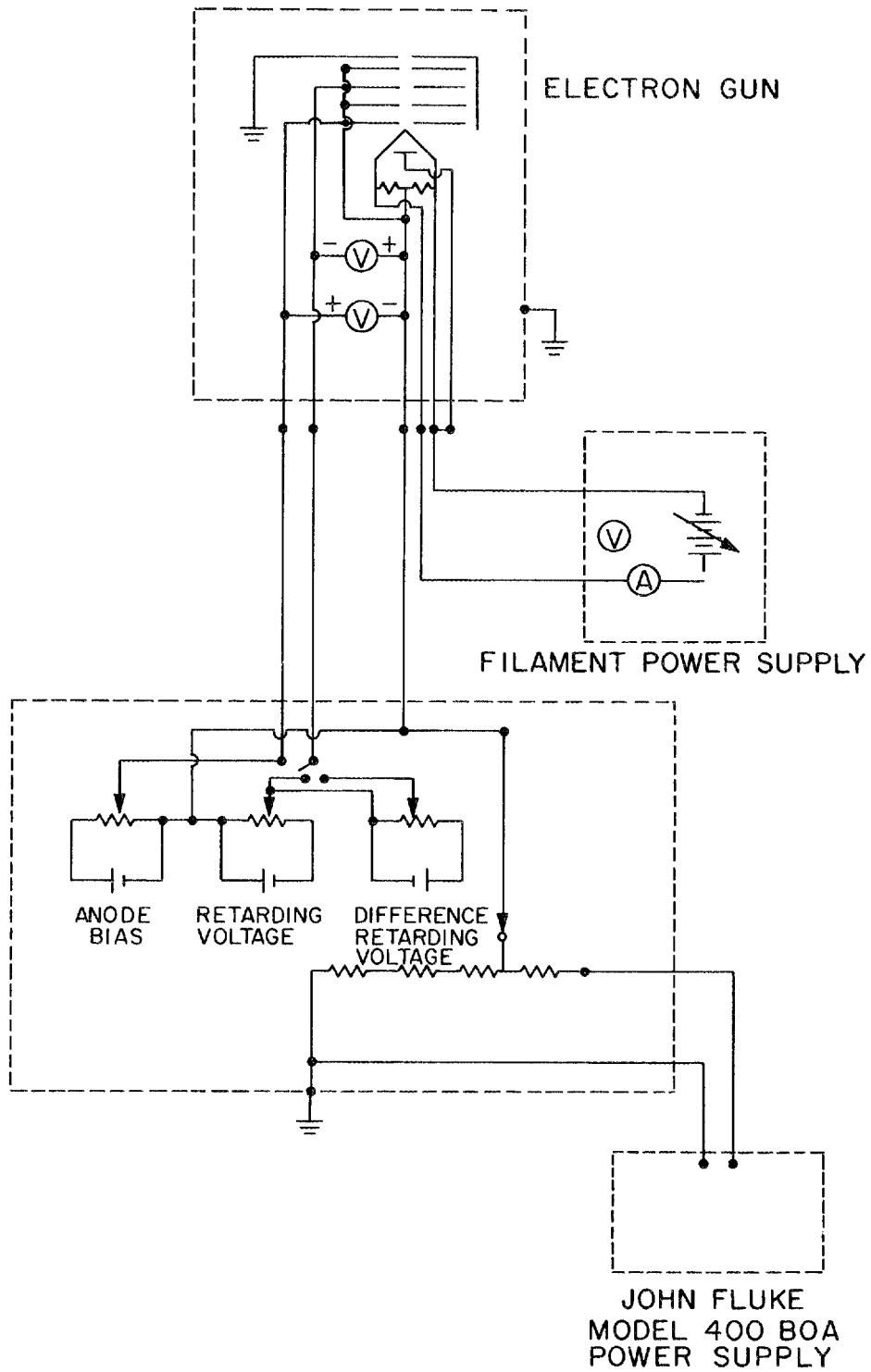


Figure 9. Electron Gun Circuit Diagram

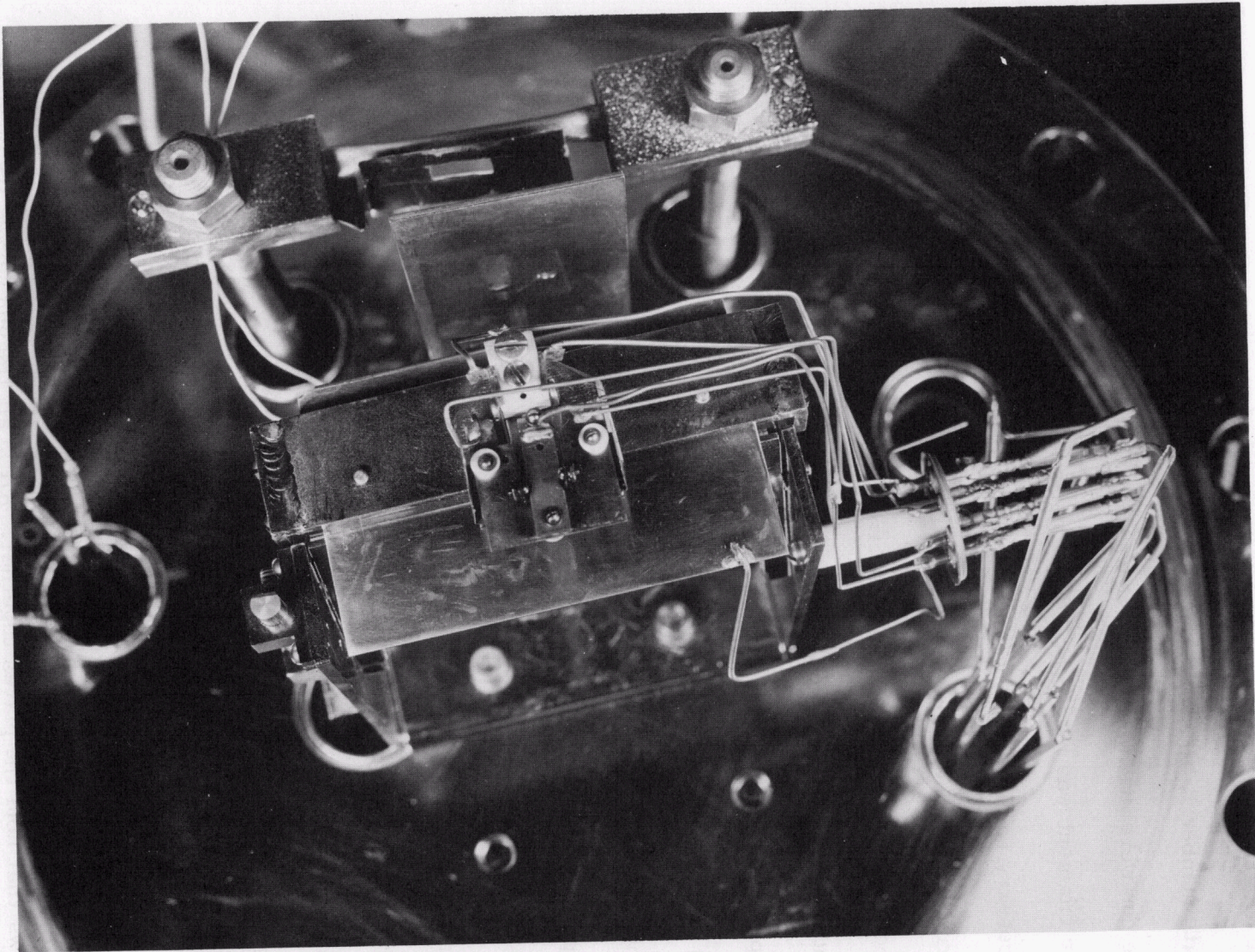


Figure 10. Photograph of Electron Gun

stainless-steel plate was placed in back of the filament and connected to the negative side of the filament (the cathode) to turn the electrons toward plate number 1, the anode. The fifth plate was grounded. All spacers in the gun were machined of lavite and fired to harden and to reduce outgassing. The filament was made of 5 mil tungsten wire. Before using the gun, it was necessary to allow it to warm up for approximately $1\frac{1}{2}$ hours to permit the current from the filament to become stabilized. It was noted that if this procedure was neglected, the electron energy of the gun varied enough to render unreliable readings. Normal current through the filament was 2.5 amperes at a potential of 2 volts. The energy range of this gun was from 1.0 e.V. to 3 k.e.V. The higher value was limited by arcing that took place between the feedthrough terminals. Power for the accelerating voltage was supplied by a John Fluke power supply, model 400 BDA. Leads were attached to the plates first by spot welding, but this was found to produce a bond of insufficient strength to withstand the necessary amount of handling to attach the gun in place. Finally, it was found that soldering with a high temperature solder would produce a good bond that could be cleaned so that outgassing was negligible. The only other problem encountered in using the gun was the alignment of the plates after disassembly to replace a filament. This difficulty was resolved by the use of two aligning pins placed in the holes in the back of the gun and by placing small ceramic tubes over the screws that hold the plates together. All in all the gun served its purpose very well; however, its energy spread was not as narrow as had been hoped.

This was perhaps due to the fact that the beam was not pulsed as described by Compton et al. (1966) nor was a magnetic focussing field present as called for in the original design.

Current Measuring System

Previous work indicated that the current in the electron beam should not exceed 10^{-7} amps and that the exposure time of the beam to the target should be as short as possible to reduce heating. These stipulations required that the current measuring device have a high sensitivity and a fast response time. The resistivity of the aluminum oxide dielectric was found to be of the order of 10^6 ohms; therefore, the input impedance of the current measuring system had to be much less than this figure. A system which met all of these requirements was two Philbrick model P2 solid state differential operational amplifiers, a Vidar model 510 integrating digital voltmeter, and a Vidar model 260 voltage-to-frequency converter. These were connected as shown in Figure 11. The two amplifiers were operated in a closed loop so that the input currents from the foils were converted to output voltages. Suppose we require a current of 10^{-7} amps., I_1 , to give an output voltage of 10 millivolts, V_o (that is, allow a current of 10^{-7} amps. to produce a full-scale deflection of 10 millivolts). Then the required feedback resistance, R_f , is given by the relationship

$$R_f = V_o / I_1 \quad . \quad (14)$$

Here R_f represents the feedback resistance, V_o the output voltage, and I_1

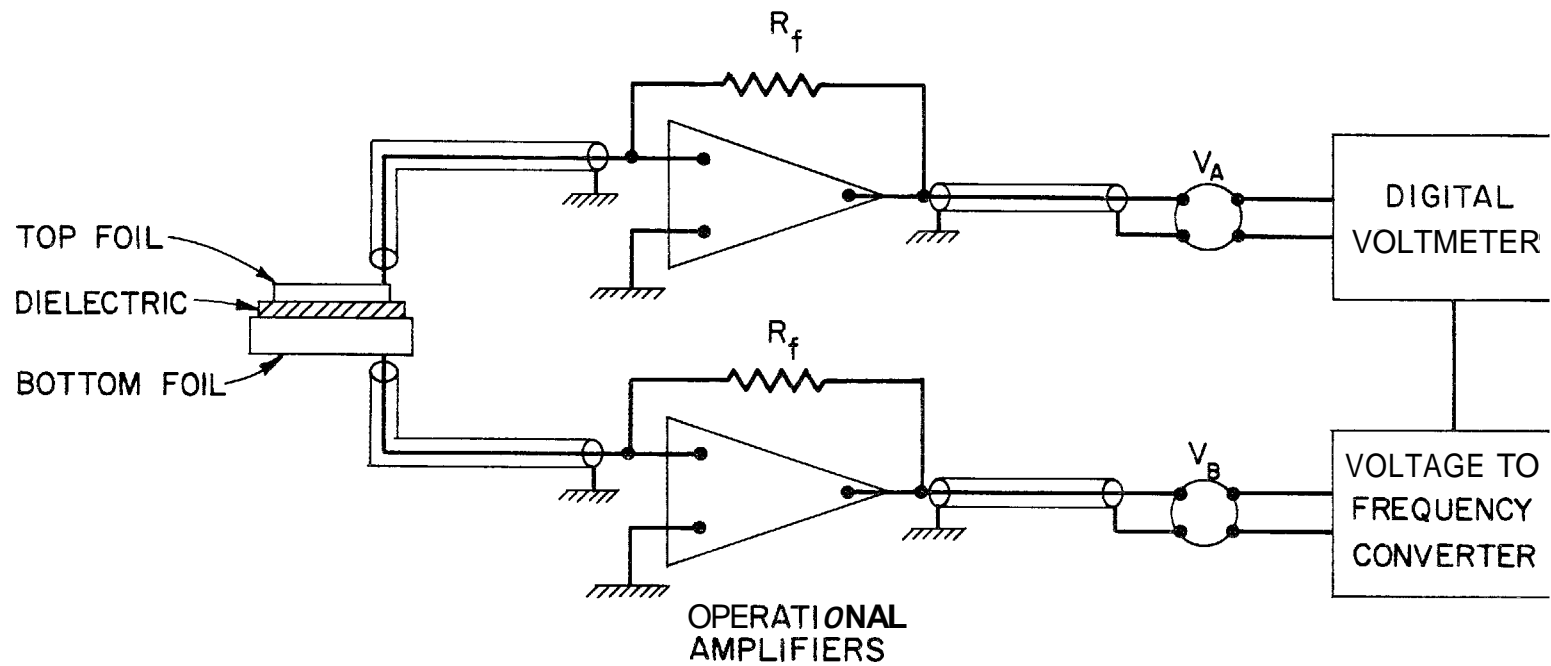


Figure 11. Schematic Diagram of Current Measuring System

the input current. From this relation, we can see that the value of R_f is 10^5 ohms. The input impedance (R_i) of the Philbricks is given by the following relations

$$R_i = V_i / I_i \quad (15)$$

and

$$A = V_o / V_i \quad (16)$$

Here V_i is the input voltage with respect to ground, V_o is the output voltage with respect to ground, I_i is the input current, and A is the amplifier gain. If the maximum output voltage is $V_o = 10^{-2}$ volts while I_f , 10^{-7} amps. and A is approximately 10^5 , then the input impedance is 1.00 ohm. This requirement for input impedance is well within the range of the P2 Philbrick amplifier. The current from the top foil, I_1 , is directed to one of the P2 amplifiers where it is converted to the voltage which is proportional to the current received (see Figure 12). This voltage is fed to the internal voltage-to-frequency converter of the Vidar 510 integrating digital voltmeter. Here it is converted to a frequency which is also proportional to the initial current. Next, this frequency goes to the scaler of the Vidar 510 integrating digital voltmeter. The current from the bottom foil, I_2 , is fed into the second P2 amplifier where it is converted into a voltage which is proportional to the current, I_2 . This voltage is then fed into the external Vidar 260 voltage-to-frequency converter where it is converted into a frequency, proportional to the current, I_2 . This frequency goes to the preset count scaler of the integrating digital voltmeter where it controls a variable time

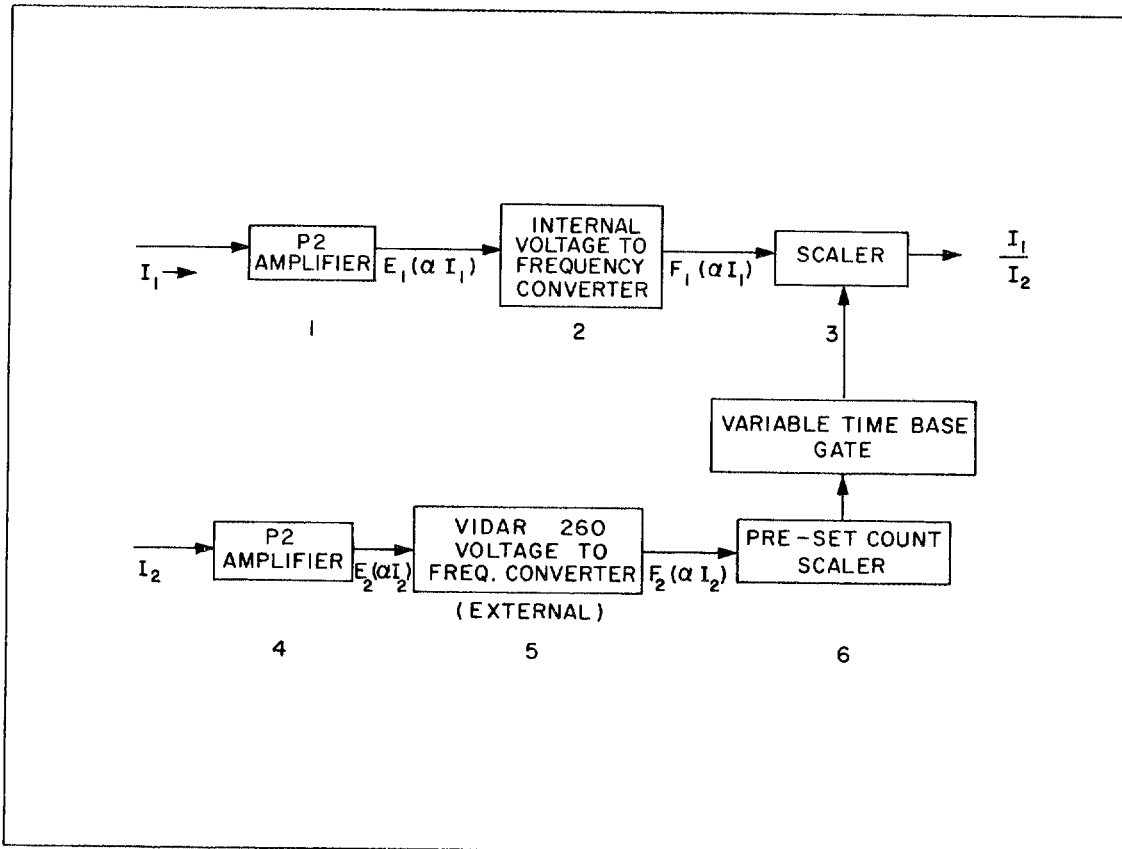


Figure 12. Operational Diagram for Ratiometer

base gate. By thus regulating the amount of time for which the scaler scans the frequency, F_1 , from the top foil, we receive a ratio of the currents leaving the top and bottom foils.

The unity gain band width for full output is 1.5 kHz, i. e., the response time is less than 1 millisecond. The amplifiers are electrically and mechanically shielded, thermally insulated, and have high linearity and low leakage currents. After 200 hours warm-up time, the drift was guaranteed to be less than 200 microvolts per month.

The Vidar model 260 converter has 10^5 ohms input resistance with input voltage of 10 millivolts and a full-scale sensitivity from 5 millivolts to 5 volts. The accuracy of each scale is better than 0.05%. The converter has an accuracy of within 0.10% of the final value after 200 microseconds. The Vidar model 510 digital voltmeter has the input impedance of 10^5 ohms at 100 millivolts. Full-scale sensitivity was from 10 millivolts to 100 volts with an accuracy greater than .015% on any scale in a 5-digit readout. The time-base gate was variable with preset count options of 10^3 , 10^4 , 10^5 counts. Thus, the Vidar model 510 digital voltmeter, the Vidar model 260 voltage-to-frequency converter and the Philbrick P2 amplifiers meet all the requirements placed upon the current measuring devices.

Secondary Electron Suppressor Assembly

To investigate the role played by secondary electrons in this experiment, we decided to incorporate a suppressor assembly into the apparatus

which would allow varying amounts of secondary suppression. The assembly took the form of two stainless-steel plates containing small apertures and separated by two 2mm-thick lavite spacer-washers. The first plate, that first encountered by a primary electron on its way toward the target from the electron gun, was grounded. Its aperture was sufficiently small to completely shield the edges of the aperture in the second plate from the primary beam. The second plate (that next to the target) was the one to which the appropriate biases were applied. The assembly was positioned near the film (second plate 2 mm from target surface) by mounting it on the target holder. Again two lavite spacer-washers were used to electrically insulate the second plate from the grounded holder.

When the bias was to remain constant during a complete investigation, the bias voltage was provided by a Keithley model 240 regulated voltage supply with an accuracy of $\pm 1\%$ or .1 volt. When the final bias was to be ten volts more positive than the cathode, the bias was obtained by tapping the accelerating voltage and adding to it a positive ten volts by means of two 8.1 volt mercury batteries and a potential divider.

III. PROCEDURE

Target Preparation

It was necessary to have a supporting substrate for the non-self-supporting film. Kodak projector slide cover glasses 8.3 cm. x 10.2 cm. were wrapped in Scotch brand masking tape and sawed to a size of 5 cm. x

10.2 cm. The wrapping procedure was performed to prevent scratching of the surface of the substrate. These glass plates were then cleaned with a solution of Knox-70 Laboratory Glass Cleaner and flushed with distilled water. The plates were then placed in a chromic acid mixture of potassium dichromate and sulfuric acid for a period of not less than 24 hours. Just prior to insertion into the vacuum deposition system, the plates were removed from the mixture and flushed with distilled water for about 30 minutes. This process cleaned the glass very well; that is, after this procedure was initiated, there was not a single case in which the film came loose from the substrate during the anodizing procedure. After flushing with distilled water the plates were placed in a vacuum desiccator and left until thoroughly dry. When dry the plates were removed from the desiccator and placed in the standard 12-inch bell jar vacuum evaporator. Here they were cleaned again by ionic bombardment for a period of from 3-5 minutes at a pressure near .05 torr. This system was then pumped down to operating pressure of 2×10^{-6} torr. At this pressure and with a mechanical shield in front of the substrate, the aluminum containing boat was outgassed. The shield was removed, the evaporating mask was placed between the substrate and the boat, and the evaporation was made. In previous work it had been necessary at this time to remove the film from the vacuum evaporator, anodize the aluminum, and then place it back in the vacuum evaporator to evaporate the silver-manganese electrical contacts. This step was eliminated, however, by changing the shape of the bottom film. With the bottom

film in the shape as shown in Figure 13, it is possible to lower the film into the anodizing solution without contaminating the solution with the silver-manganese.

After the bottom layer had been evaporated on the glass, the silver manganese contacts were evaporated onto the substrate in the same vacuum system. The glass substrate and the bottom film were removed from the vacuum evaporator and placed in the anodizing apparatus shown in Figure 14. The anodizing solution is a 3% solution by weight of tartaric acid in distilled water with a pH adjusted by ammonium hydroxide to 5.5. For this arrangement Hass (1949) reported that a linear relationship between the oxide thickness and the applied voltage existed. However, more recent work by Garber (1965) and Holland (1961) showed that this relationship is not linear. Their work is indicated in Figure 15. Using a General Radio Company Impedance Bridge type 1650-A, the capacitance of the target can be measured. From the capacitance the thickness of the dielectric can be calculated. The dielectric constant is taken to be 8 [Hartman and Chivian (1964)]. The relation between capacitance and thickness is:

$$T(\text{\AA}) = \frac{\epsilon 8.85 A (\text{cm.})^2}{C(\mu\text{f.})} \quad (17)$$

Here T is the thickness in angstroms, ϵ is the dielectric constant relative to vacuum, C is the capacitance in microfarads, and A is the area in cm.^2 of the dielectric. It has been shown in previous work [Garber(1965)] that a 75 \AA thick aluminum oxide dielectric gives sufficient insulation for this work. To insure that the dielectric was of good quality, the plate was left

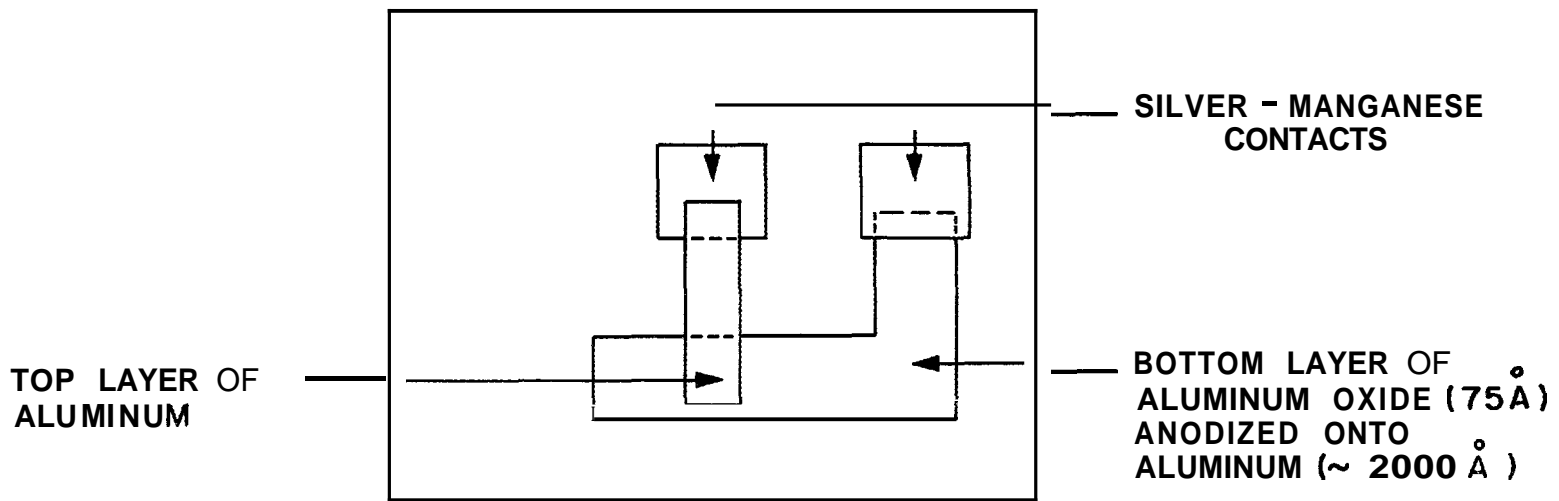


Figure 13. Top View of Sandwich

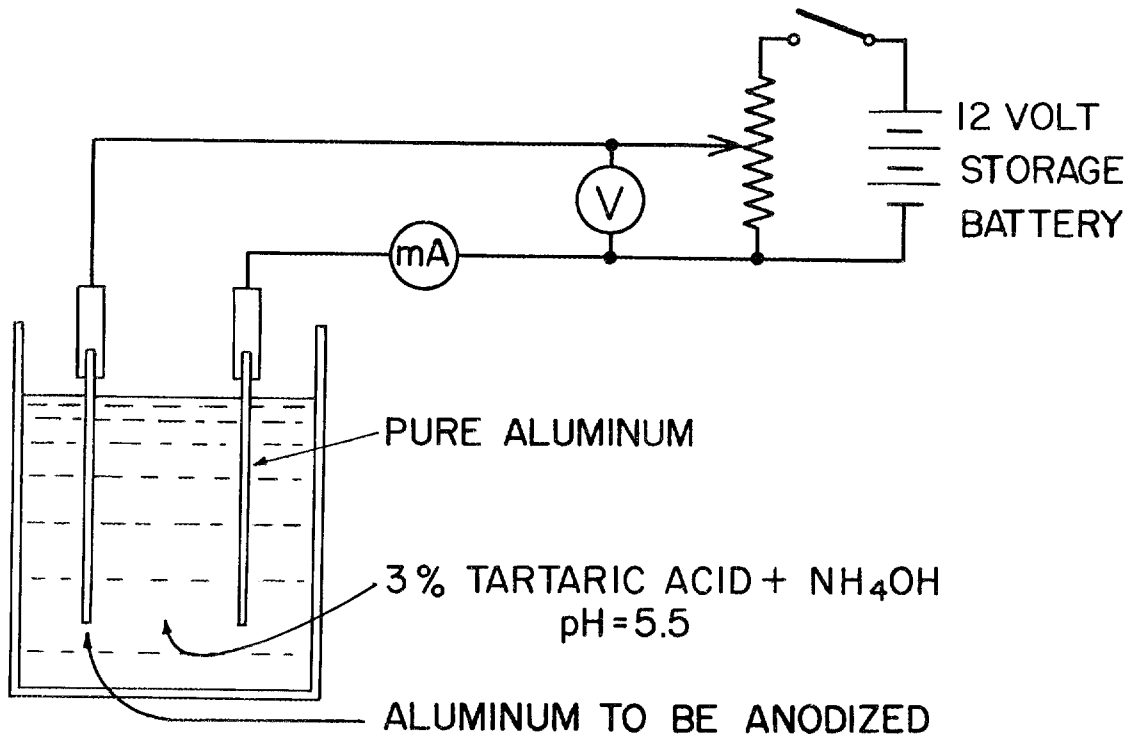


Figure 14. Schematic Diagram of Anodic Oxidation Apparatus

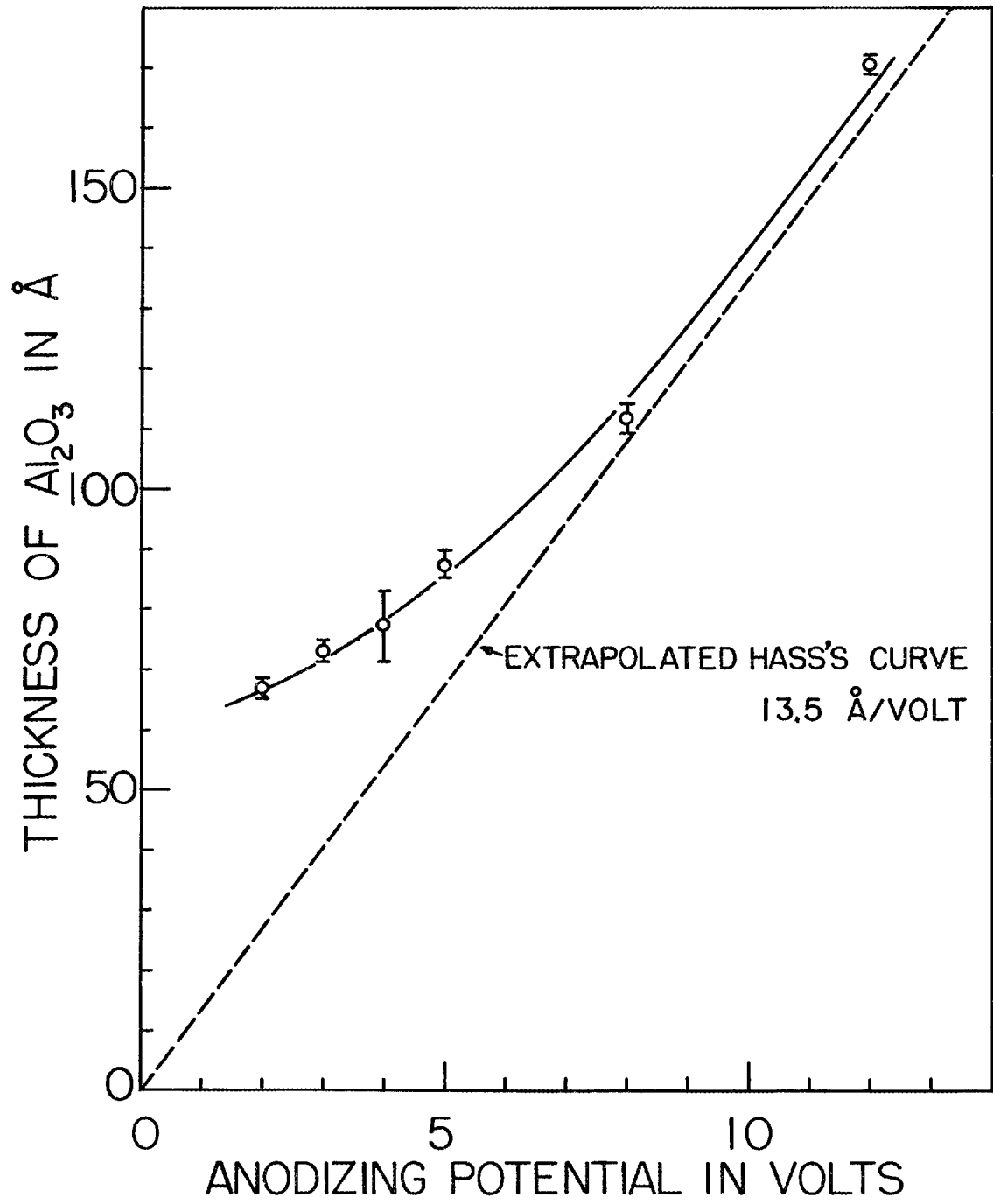


Figure 15. Oxide Thickness Versus Applied Voltage

in the anodizing solution for a period of 5 minutes. After removal, the plate was flushed with distilled water to remove the electrolyte and was degreased with isopropyl alcohol. The plate was next dried in a vacuum desiccator. Next the leads were soldered to the silver manganese contacts by means of a low temperature solder. During this procedure the bottom film and dielectric were shielded by means of a paper shield to prevent any contamination, e.g., solder droplets. At this point any contamination would puncture the dielectric and a short would result when the top film was evaporated. The substrate was then placed in the rotating holder, shown in Figure 7, in the vacuum system, and the system was closed. To obtain proper operating pressures, the system was baked out at a temperature of 200°C for a period of from 12 to 24 hours. The baking procedure was not observed in the instances when the system was to be opened before observations were taken to allow placement of the secondary electron suppressor assembly. After baking, the system was cooled, the gun filament was heated, the mechanical shutter was closed and the outgassing procedure for the evaporation source was performed. After outgassing the shutter was raised, and the material for the top layer was evaporated. The target was then rotated to the proper angle. If a target was to be observed with varying degrees of secondary suppression, the system was then opened and the suppressor assembly was installed.

A completed target is shown in Figure 16. Thickness was monitored during evaporation using a calibrated Speedivac film thickness monitor.

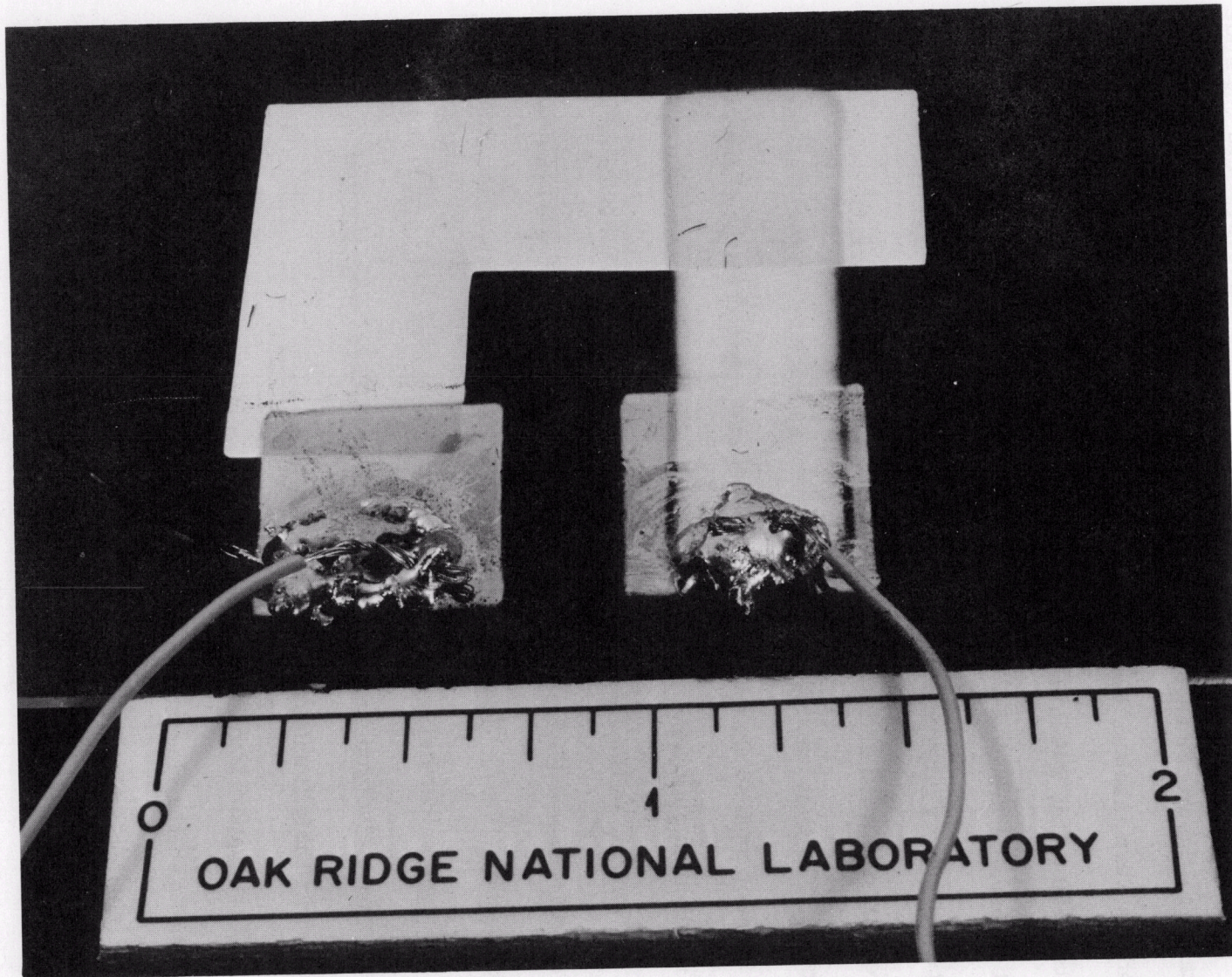


Figure 16. Photograph of Completed Target

Experimental Procedure

After the gun had been warmed, the top layer evaporated and the slide rotated to the proper angle, the accelerating voltage was set at 1.0 e.V. Readings were taken at 1 volt intervals from 1 volt to 20 volts. From 20 volts to 50 volts, 2 volt intervals were taken and from 50 to 100 volts, 5 volt intervals were taken. Twenty volt intervals were used from 100 to 500 volts and 50 volt intervals from 500 to 1000 volts. Thereafter the intervals were 100 volts until the energy required for complete penetration was reached. The evaporating mask in the ultrahigh vacuum system was made in the form of an L so that when the sandwich was rotated to the chosen angle, the mask could also serve as a bias plate.

The bias on the L-shaped bias plate during electron bombardment of the target was usually five volts negative, a figure suggested by previous work [Garber (1965)]. It was desired to investigate the effect of various bias voltages on the current ratios. This investigation was carried out using the secondary electron suppressor assembly. Voltages were applied as indicated in Table II unless otherwise specified.

This evaporation mask also served as an electronic shutter to prevent the beam from the electron gun from striking the target continuously. The rotating switch, circuit diagram in Figure 17, was connected so that when the switch is turned to the off position the bias applied to the bias plate was 1500 volts negative or larger. This prevented the electron beam from reaching the film. When the switch was in the on position the plate was

TABLE II

SECONDARY ELECTRON SUPPRESSOR ASSEMBLY BIAS VOLTAGES

Bias Plate Voltage	Primary Electron Energy, E, in e. V.
Grounded	1
"	2
.	.
.	.
.	.
-1	10
-2	11
-3	12
-4	13
-5	14
-6	15
-E+10	16

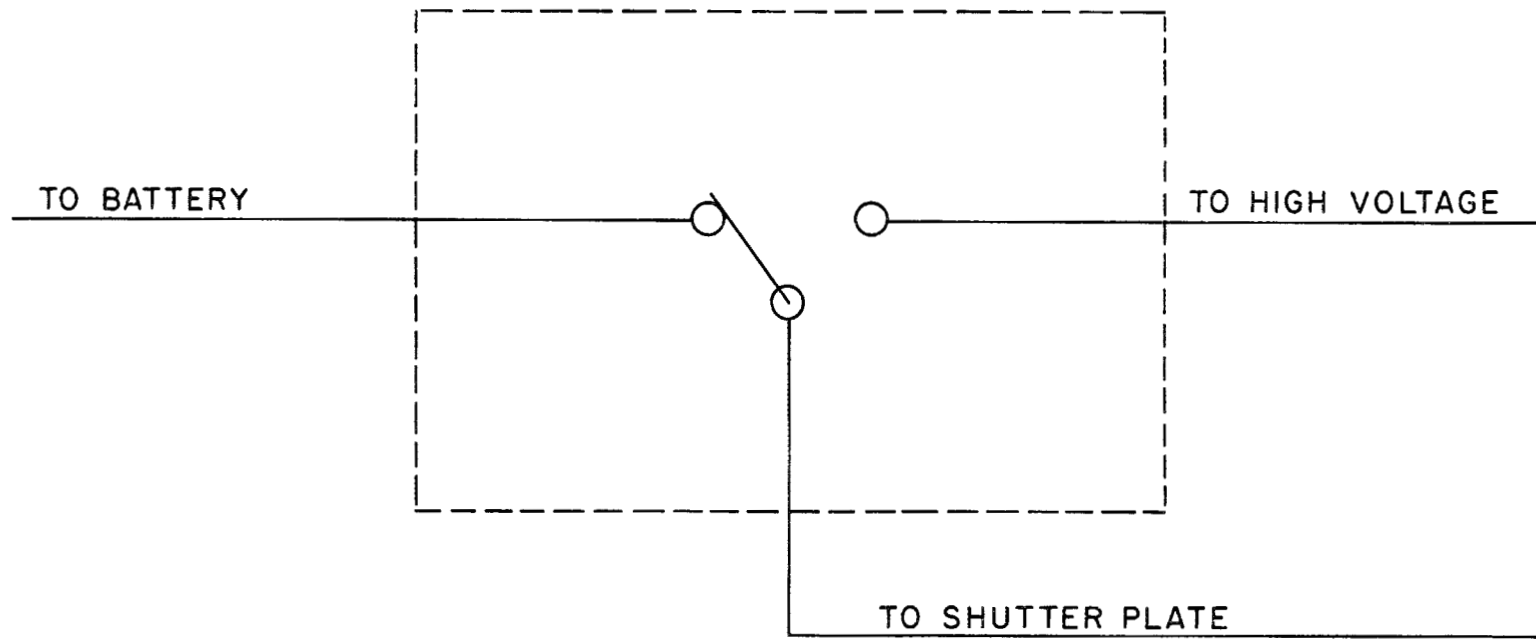


Figure 17. Circuit Diagram of Rotating Switch for Electronic Shutter

biased as shown in Table II. After an accelerating voltage was set, the rotating switch was turned so that the bias was on the plate. The counting interval on the scaler was turned on. When the scaler ceased counting its activating switch was turned off to prevent a second count and the rotating switch was turned off so that the electronic shutter was activated. The ratio was noted and then another accelerating voltage was set. The previous reading was then recorded. This method allowed a short time for equilibrium to be attained before a second reading was taken. The setup described previously in the current measuring system provided a means for measuring the ratio of the bottom current to the current in the top foil. Let B represent the current in the bottom layer and T the current in the top layer. The ratio was then B/T. The following equation shows the relationship between B/T and the quantity plotted on the following graphs, $T/B + T$

$$1/\left(\frac{B}{T} + 1\right) = \frac{T}{B + T} \quad (18)$$

This ratio $T/(B + T)$ is plotted on the linear axis of semi-log paper against the energy in electron volts on the logarithmic axis.

CHAPTER IV

RESULTS AND DISCUSSION

Figure 18 presents a graph of the ratio of the current collected in the top layer of the Al-Al₂O₃-Al diode to the total current impinging upon it for various bias voltages and taken under 10⁻⁶ torr vacuum conditions. The curve representing the situation using -E + 10 V. bias shows a rising current to the top layer in the lower energy region (< 100 e.V.). This may be explained by a decrease in the mean free path with increasing primary energy. The order of magnitude of the attenuation length for electrons with primary energy less than those at which the top current becomes constant may be determined as follows. We may use the equation

$$F_2 - F_1 = e^{-\frac{t}{L}} \quad ,$$

where F_1 is the ratio of top current to total current at the energy of interest; F_2 is the corresponding ratio at the energy where the top current becomes constant; t is the thickness of the top layer in angstrom units, and L is the attenuation length. A graph of the attenuation length for the 180 Å foil versus energy with bias (-E + 10) is presented in Figure 19.

The region of the -E + 10 V. biased curve of Figure 18 in which the current to the top layer is constant (60 e.V. to 500 e.V.) demonstrates that at these energies there is no electron transport taking place across the top layer and through the insulator.

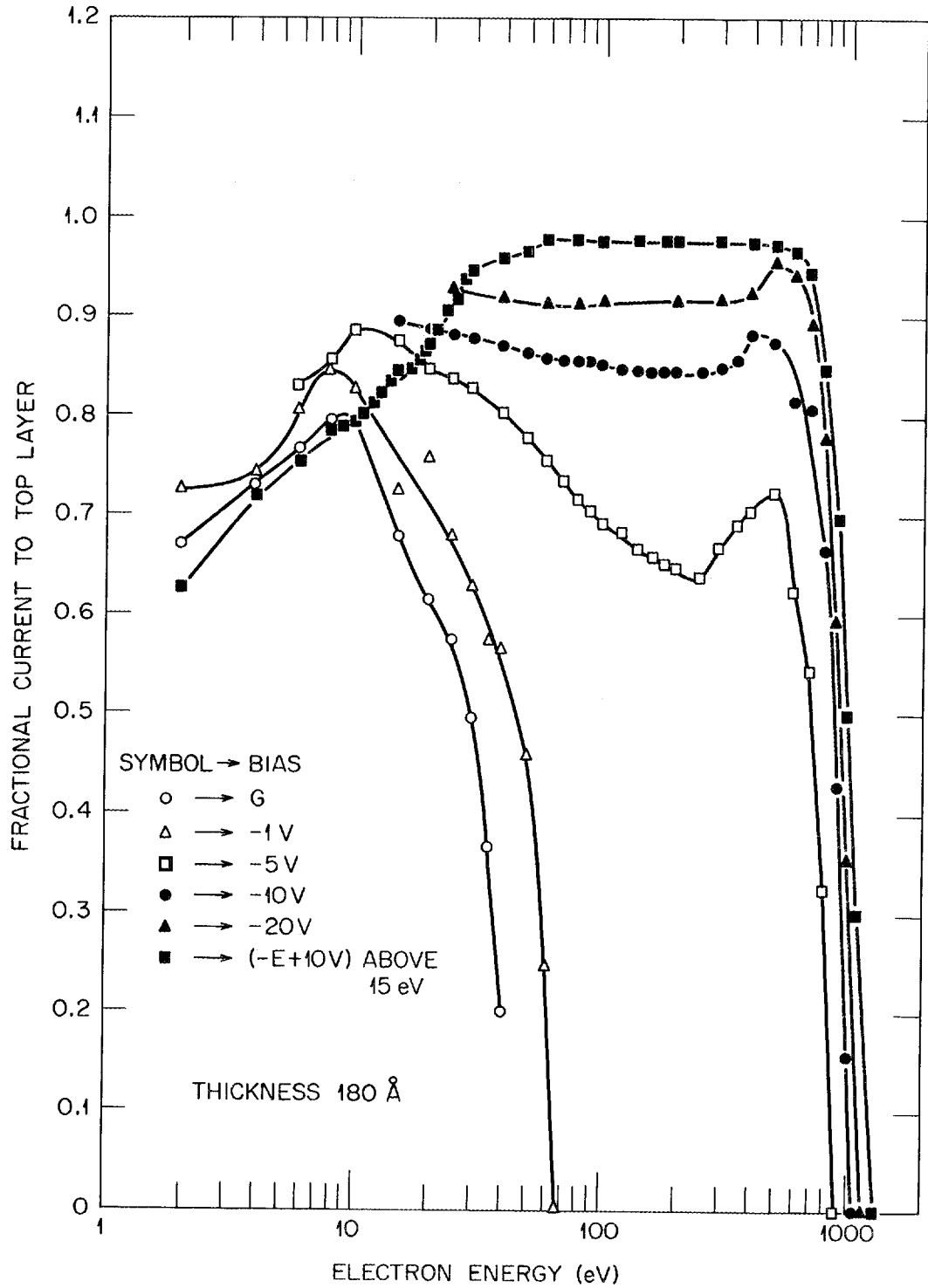


Figure 18. Top Current as a Function of Incident Electron Energy for a 180 Å Thick Aluminum Foil with Various Bias Voltages

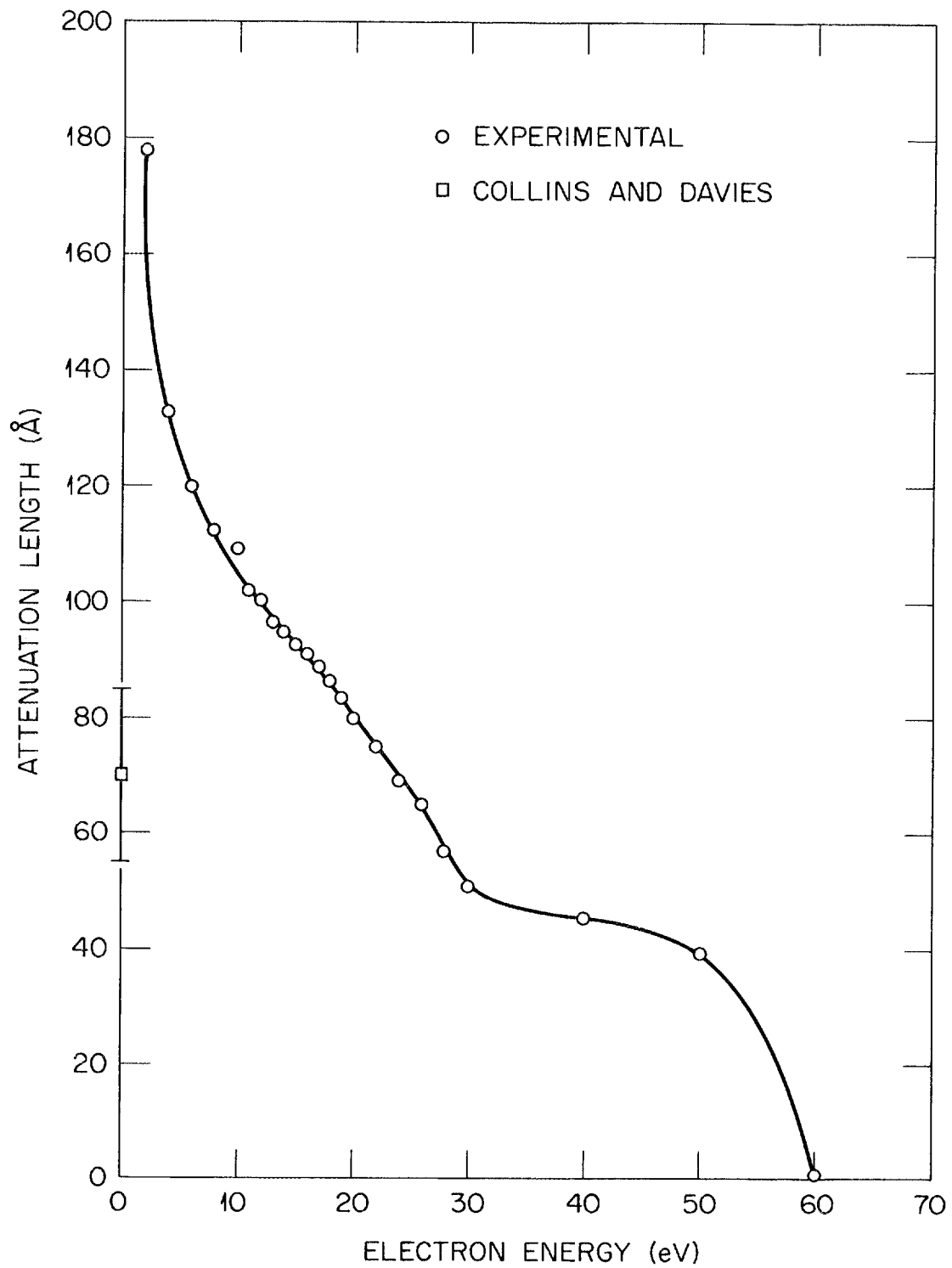


Figure 19. Attenuation Lengths in Aluminum for Electrons of <60 e.V. Energy

The third region, that above 500 e.V., shows an increasing penetration of the top layer. From this region of the curve one could calculate stopping powers. This has been done by previous investigators [i. e., Garber (1965)]. For a comparison of theoretical and experimental data of such investigations, refer to Figure 2.

Figures 20-25 give data taken under ultrahigh vacuum conditions ($\sim 10^{-9}$ torr) using a bias of five volts negative. As is noted, observations were made for various angles of incidence. In the low energy region (< 60 e.V.) we notice that the current to the top layer increases as the angle of incidence increases. This is in qualitative agreement with predictions [Ritchie (1957)] that the probability of surface plasma interactions should be enhanced as the reciprocal of the cosine of the angle of incidence.

For the second region, 60 e.V. to 500 e.V., we note that the ratio of the top current to total current is not as high as for a similar region of the curve in Figure 18 using $-E + 10$ V. bias. This fact leads us to conclude that there has been a decrease in top current due to secondary electron emission from the top layer. In the vicinity of ~ 150 e.V. the curves representing the various angles cross. After crossing, the curve for the greater angle is lower. This may be explained in accordance with Bruining's experiments (1936) which showed that above 100 e.V. more secondary electrons were produced from a smooth metallic film as the angle of incidence of the primary beam was increased. According to Bruining, a high energy electron which could travel some distance in the layer would do so and liberate secondaries.

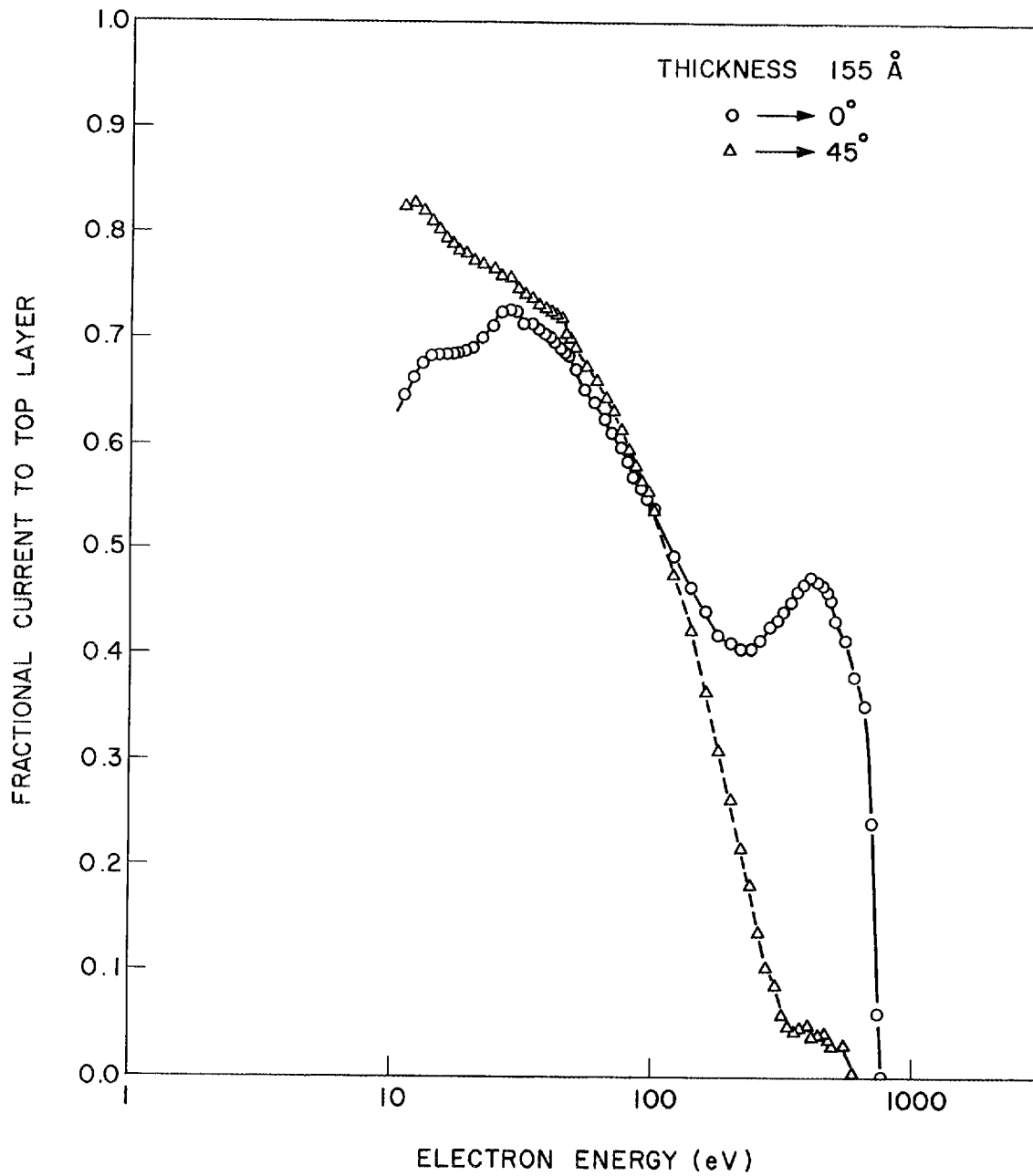


Figure 20. Top Current as a Function of Incident Electron Energy for a 155 Å Thick Aluminum Foil at Incident Angles of θ and 45 Degrees

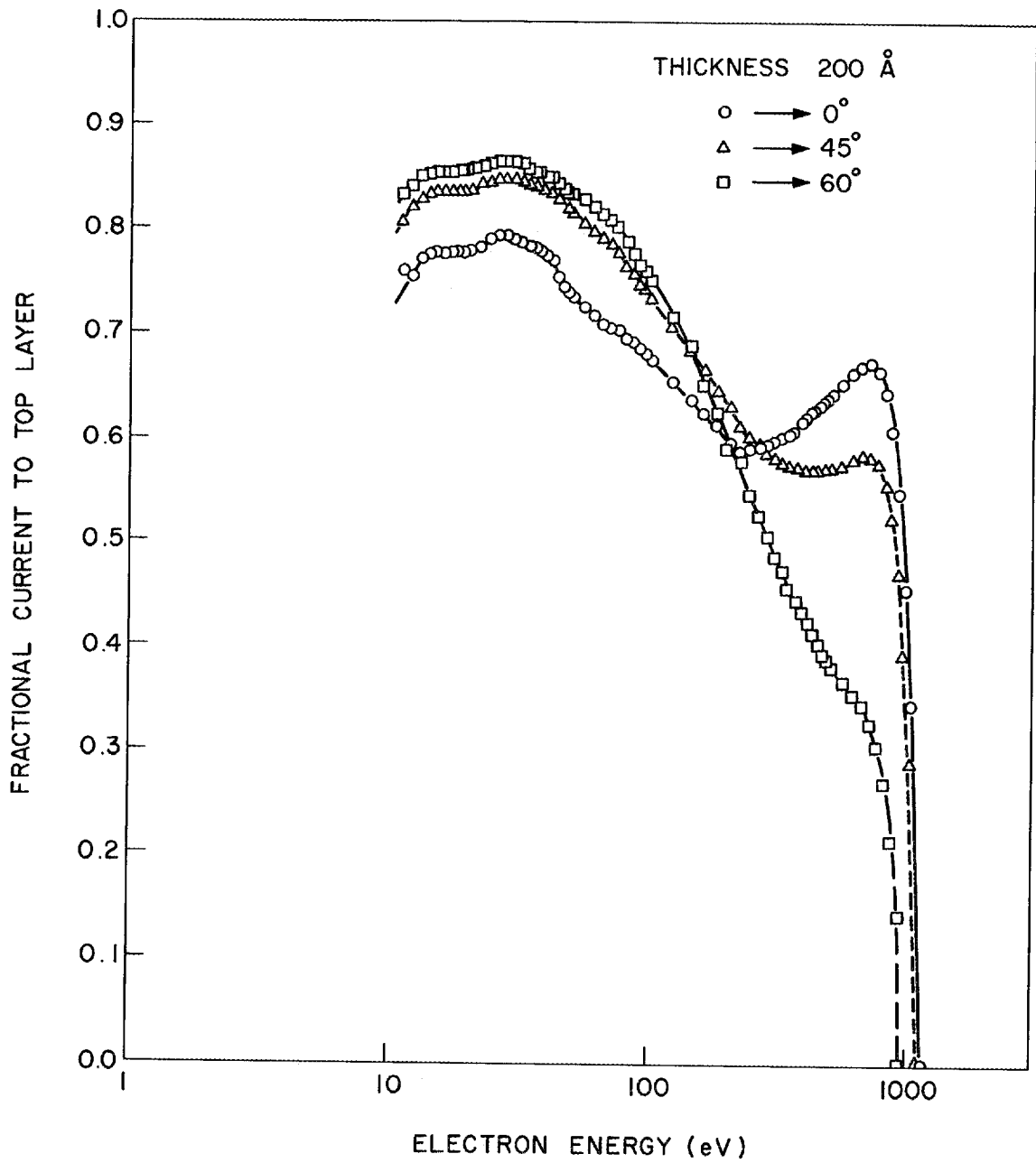
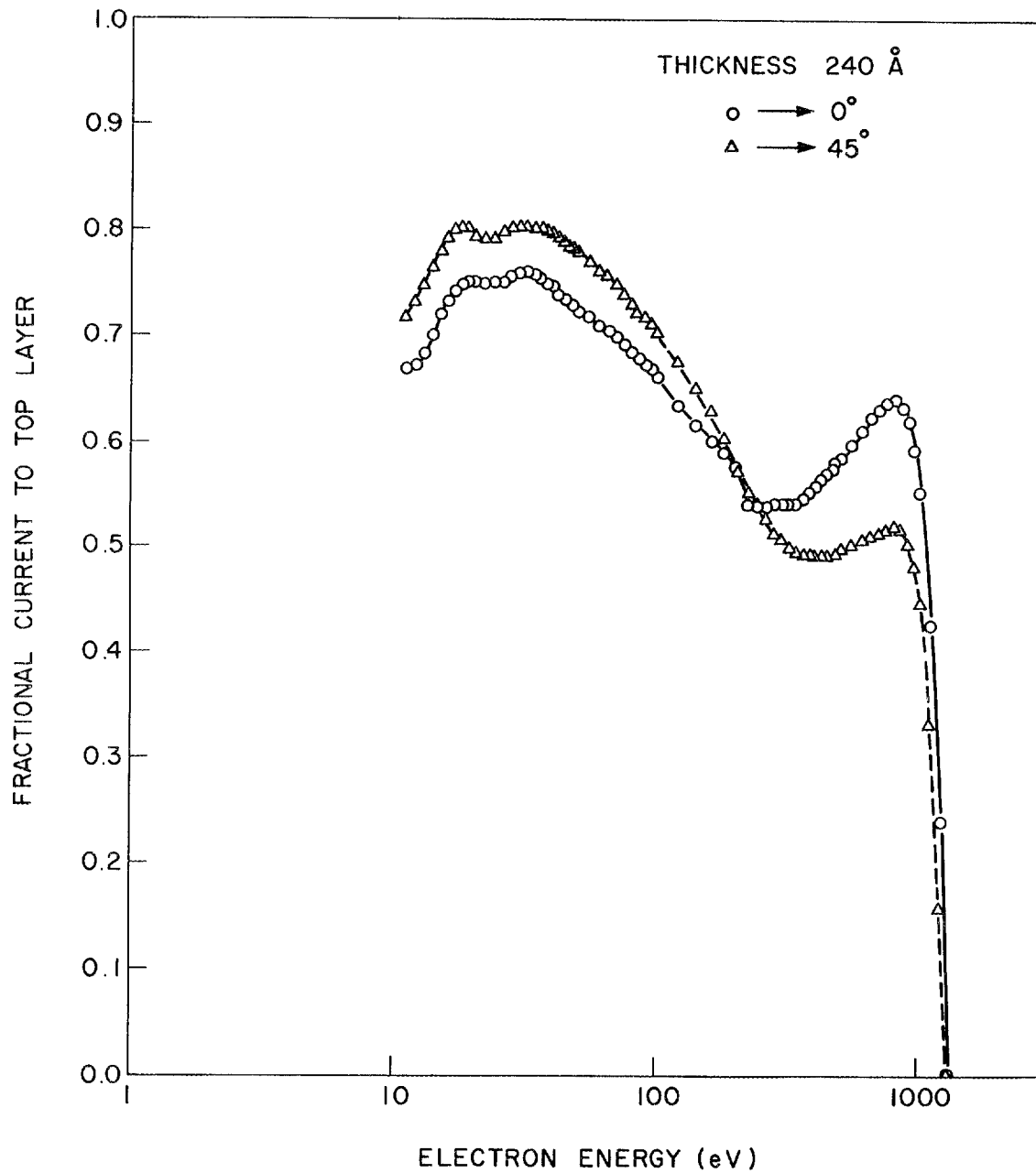


Figure 21. Top Current as a Function of Incident Electron Energy for a 200 Å Thick Aluminum Foil at Incident Angles of 0, 45, and 60 Degrees



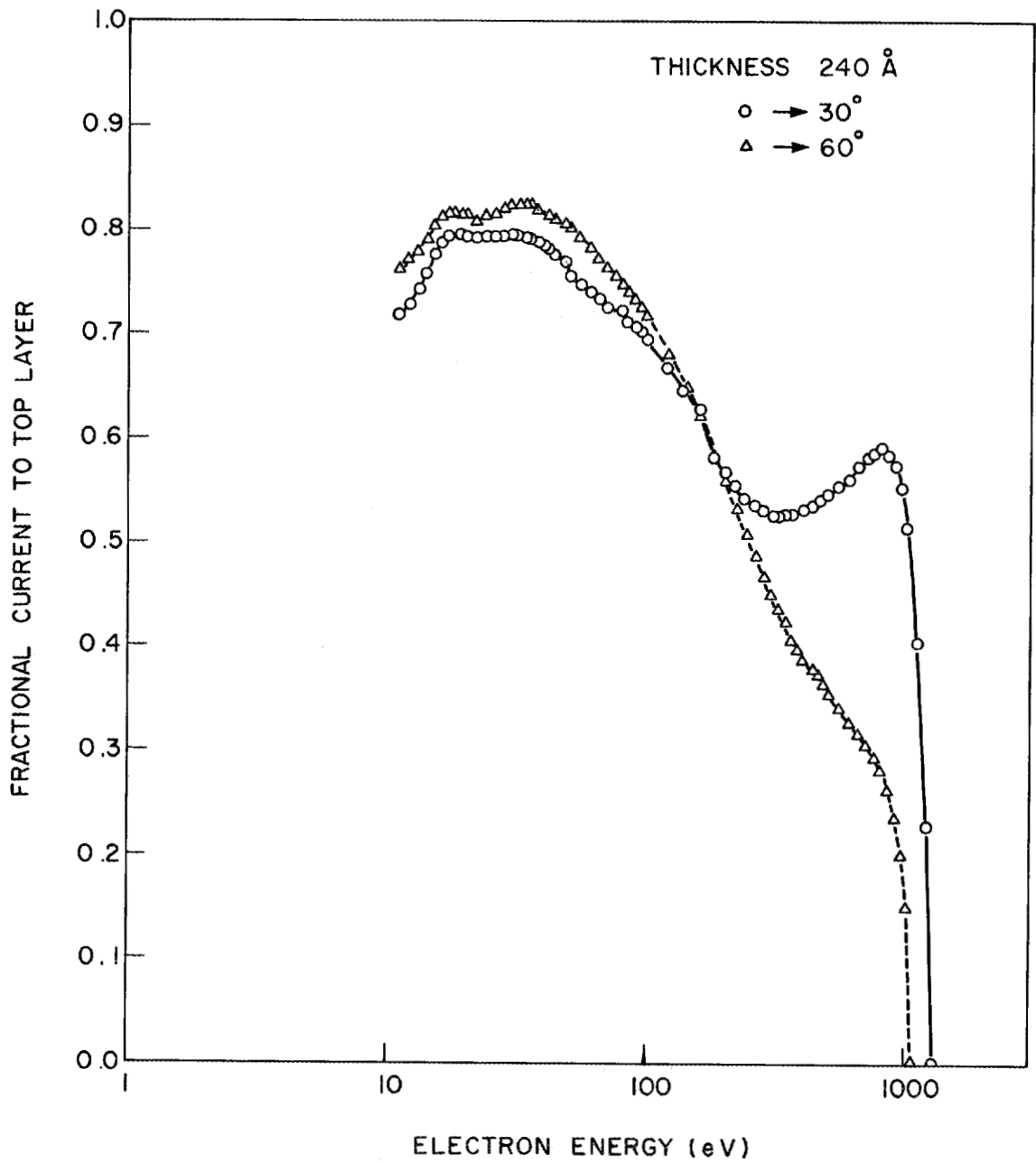


Figure 23. Top Current as a Function of Incident Electron Energy for a 240 Å Thick Aluminum Foil at Incident Angles of 30 and 60 Degrees

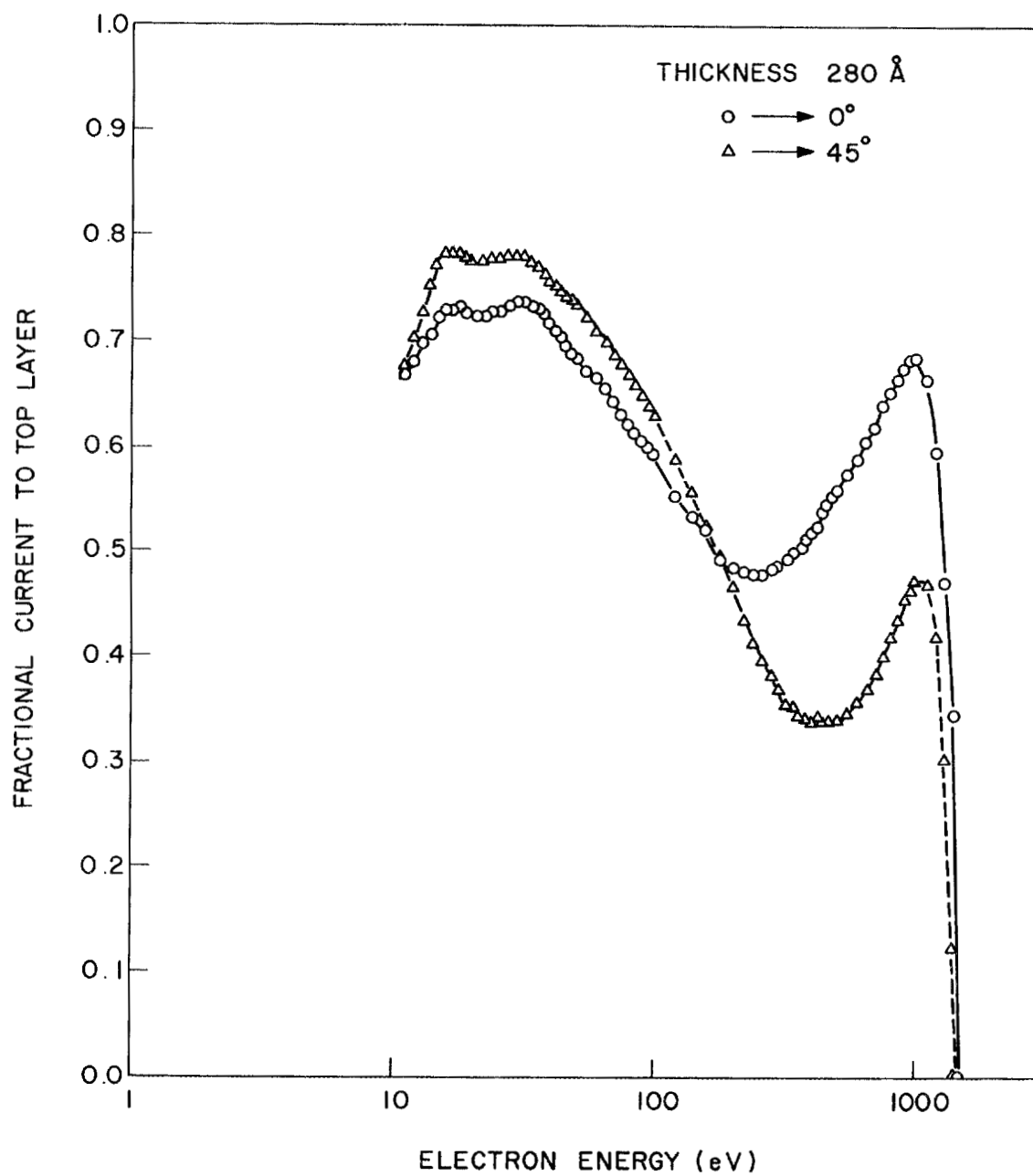


Figure 24. Top Current as a Function of Incident Electron Energy for a 280 Å Thick Aluminum Foil at Incident Angles of 0 and 45 Degrees

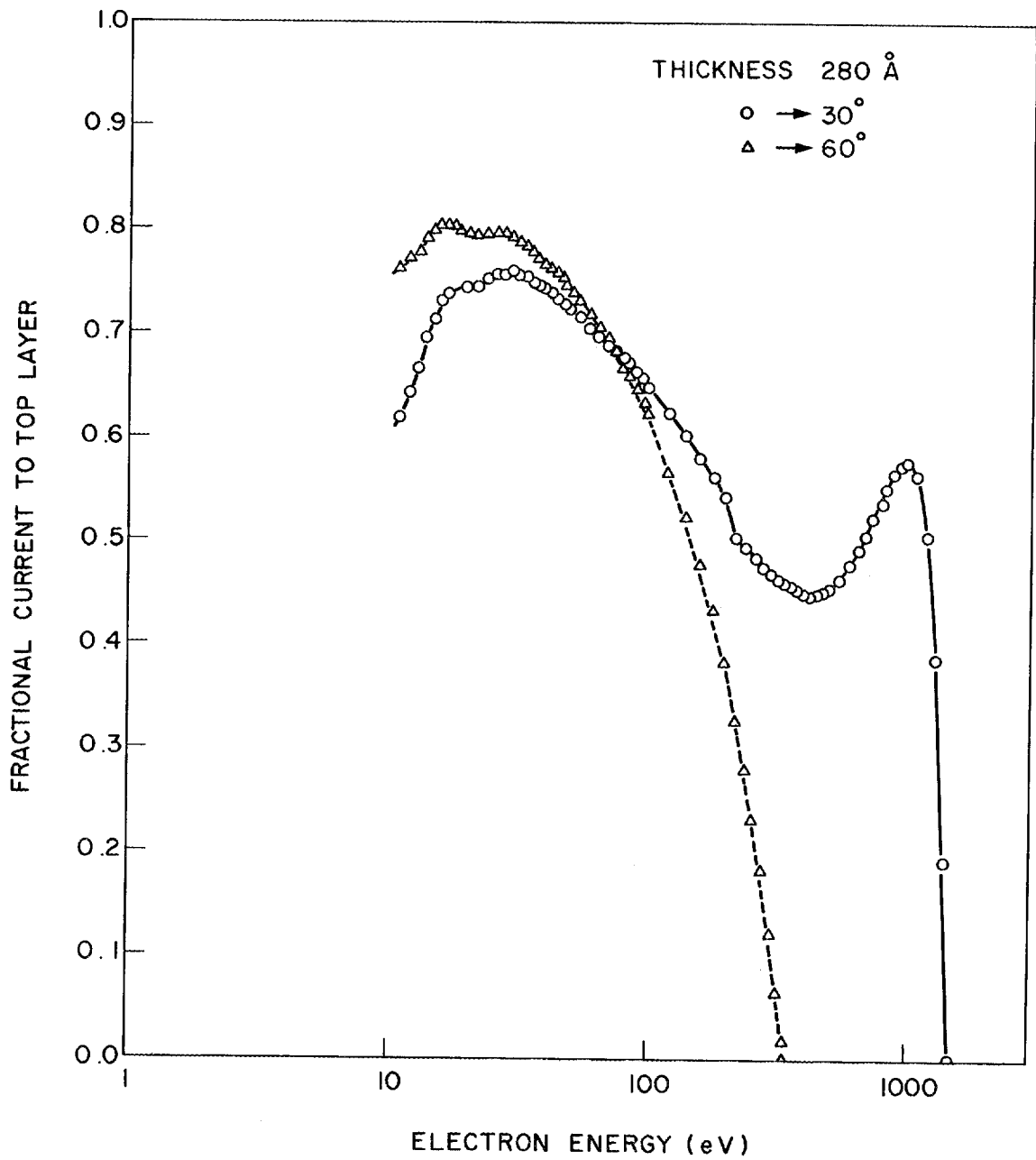


Figure 25. Top Current as a Function of Incident Electron Energy for a 280 Å Thick Aluminum Foil at Incident Angles of 30 and 60 Degrees

However, these secondaries had a shorter distance to travel to the surface than they would had the primary been normally incident on the surface. After 150 e.V. to 200 e.V., we note a rise and peak in the curve which we may interpret as follows. As a beam is impinging on the target, some primary electrons will form secondaries that may be lost unless properly suppressed. Now if the energy of the primary is such that an L-shell interaction may occur, primaries which would otherwise create secondaries now interact with the L-shell. Thus there is a resulting increase in the top current since many secondaries which were being lost are not now even formed. It must also be noted that as the angle of incidence increases the peak due to L-shell interaction decreases. Here the interpretation may be again that the secondaries which are formed now have a shorter distance to travel to reach the surface and thus escape.

The final region of the curve, that above 500 e.V., shows a declining ratio indicating that penetration of the top layer is now taking place. The interpretation is the same as for the corresponding part of Figure 18.

CHAPTER V

CONCLUSIONS

This experiment divides itself conveniently into two parts: that performed in ultrahigh vacuum with incomplete suppression of secondary electrons and that performed with a target that had been exposed to air before observation but with various amounts of secondary suppression including complete suppression. A comparison of the results of the two parts permits one to conclude that the shape of the curve obtained is dependent critically upon the amount of the secondary suppression.

With complete secondary suppression, the shape of the initial part of the curve may be interpreted as a decrease in the mean free path with an increase in the primary energy. This decrease however is accompanied by an increased production of secondary electrons, and thus attenuation lengths calculated from this curve must be considered as of orientation value only.

An interpretation of the work performed in ultrahigh vacuum at normal beam incidence does not differ substantially from that in previous work. Nor does the fact that secondary electrons were incompletely suppressed alter the interpretation of the various peaks as being due to surface plasmon, volume plasmon, or L-shell interactions.

From the data without complete secondary suppression, performed in ultrahigh vacuum, one can see that there is an enhancement of the surface plasmon excitation with an increase in the angle of incidence of the primaries. One notes that the peaks obtained with incomplete secondary suppression are due to electrons which have undergone inelastic scattering in plasmon production and thus did not produce secondaries which could be lost from the top layer.

A comparison of the two curves, with and without complete suppression, permits one to conclude that the cause of the decreased probability of an L-shell interaction with an increase in the angle of incidence is the loss of more secondaries in accordance with the work of Bruining (1936).

BIBLIOGRAPHY

BIBLIOGRAPHY

- Birkhoff, R. D., "Energy Loss Spectra for Charged Particles Traversing Metal and Plastic Films," in Physical Processes in Radiation Biology. New York: Academic Press, 1964.
- Bruining, H., *Physica* 3, 1046 (1936).
- Bohm, D. and D. Pines, *Phys. Rev.* 82, 625-634 (1951).
- Collins, R. E. and L. W. Davis, *Appl. Phys. Letters* 2, 213 (1963).
- Compton, R. N., G. S. Hurst, L. G. Christophorou, and P. W. Reinhardt, "Electron Capture Cross Sections and Negative Ion Lifetimes," Oak Ridge National Laboratory Report ORNL-TM-1409 (1966).
- Crowell, C. R., W. G. Spitzer, L. E. Howarth, and E. E. LaBate, *Phys. Rev.* 127, 206 (1960).
- Crowell, C. R. and S. M. Sze, *Phys. Rev. Letters* 15, 659 (1965).
- Garber, F. W., "Low Energy Electron and Proton Transmission in Aluminum and Silver," Oak Ridge National Laboratory Report ORNL-TM-1153 (1965).
- Gryzinski, M., *Phys. Rev.* 138, A305 (1965); 138, A322 (1965); 138, A336 (1965).
- Hartman, T. E. and J. S. Chivian, *Phys. Rev.* 134, 1094-1101 (1964).
- Hass, G., *J. Opt. Soc. Am.* 39, 532-540 (1949).
- Höhler, G., ed., Springer Tracts in Modern Physics. Vol. 38, Springer-Verlag, Berlin, Heidelberg, New York (1965).
- Holland, L., Vacuum Deposition of Thin Films. London: Chapman and Hall, Ltd., 1961.
- Kanter, H. and E. J. Sternglass, *Phys. Rev.* 126, 620 (1962).
- Klemperer, O. and J. P. G. Shepherd, *Advances in Phys.* 12, 355-390 (1965).
- Marton, L., *Rev. Mod. Phys.* 172, 183 (1956).

- Marion, L., L. B. Leder and H. Mendlowitz, Advances in Electronics and Physics. New York: Academic Press, 1955, VII, 183-238.
- Mott, N. F., and H. Jones, The Theory of the Properties of Metals and Alloys. Dover Publications, Inc., New York, (1958) p. 268.
- Quinn, J. J., Phys. Rev. 126, 1453 (1962).
- Quinn, J. J., Appl. Phys. Letters 2, 167 (1963).
- Ritchie, R. H., Phys. Rev. 106, 874-881 (1957).
- Ritchie, R. H., Phys. Rev. 114, 644 (1959).
- Ritchie, R. H., M. Y. Nakai, and R. D. Birkhoff, "Low Energy Electron Mean Free Paths in Solids, " to be published in Advances in Radiobiology, Vol. III, (1967).
- Soshea, R. W., and R. C. Lucas, Phys. Rev. 138, A1182 (1965).
- Stern, E. A., and R. A. Ferrell, Phys. Rev. 120, 130 (1960).
- Stuart, R., F. Wooten, and W. E. Spicer, Phys. Rev. 135, A495 (1964).
- Walske, M. C., Phys. Rev. 101, 940 (1956).

INTERNAL DISTRIBUTION

- | | |
|-------------------------------------|----------------------------------|
| 1. Biology Library | 92. H. G. MacPherson |
| 2-4. Central Research Library | 93. K. Z. Morgan |
| 5. Reactor Division Library | 94-118. S. J. Nalley |
| 6-7. ORNL-Y-12 Technical Library | 119. D. R. Nelson |
| Document Reference Section | 120-124. R. H. Ritchie |
| 8-57. Laboratory Records Department | 125. H. C. Schweinler |
| 58. Laboratory Records, ORNL R. C. | 126. M. J. Skinner |
| 59. E. T. Arakawa | 127. W. S. Snyder |
| 60. W. B. Ard | 128. E. G. Struxness |
| 61-85. R. D. Birkhoff | 129. A. M. Weinberg |
| 86. L. C. Emerson | 130. G. M. Fair (consultant) |
| 87. R. N. Hamm | 131. J. C. Frye (consultant) |
| 88. J. A. Harter | 132. J. B. Hursh (consultant) |
| 89. H. H. Hubbell, Jr. | 133. E. P. Odum (consultant) |
| 90. C. E. Larson | 134. R. L. Platzman (consultant) |
| 91. J. L. Liverman | 135. H. C. Wyckoff (consultant) |

EXTERNAL DISTRIBUTION

136. R. Bass, Department of Physics, State College of Arkansas, Conway, Arkansas.
137. J. A. Bearden, The John Hopkins University, Baltimore, Maryland.
138. F. W. Garber, Physics Department, University of Tennessee, Knoxville, Tennessee.
139. C. J. Calbick, Components and Solid State Device Division, Bell Laboratories, Murray Hill, New Jersey.
140. V. E. Cosslett, Cavendish Laboratory, University of Cambridge, Cambridge, England.
141. C. R. Crowell, Bell Laboratories, Murray Hill, New Jersey.
142. H. Ehrenreich, Physics Department, Harvard University, Cambridge, Massachusetts.
143. U. Fano, National Bureau of Standards, Washington, D. C.
144. C. Feldman, United States Naval Research Laboratory, Washington, D. C.
145. R. A. Ferrell, University of Maryland, College Park, Maryland.
146. G. Hass, U.S. Army Engineer Research and Development Laboratories, Fort Belvoir, Virginia.
147. T. E. Hartman, Texas Instruments, Inc., Dallas, Texas.
148. L. E. Hawarth, Bell Telephone Laboratories, Murray Hill, New Jersey.
149. R. L. Hines, Northwestern University, Evanston, Illinois.

150. G. S. Hurst, Department of Physics, University of Kentucky, Lexington, Kentucky.
151. F. Hutchinson, Biophysics Department, Yale University, New Haven, Connecticut.
152. G. Jull, Imperial College of Science and Technology, University of London, London, England.
153. H. Kanter, Westinghouse Research Laboratories, Pittsburgh, Pennsylvania.
154. J. Kastner, Argonne National Laboratory, Argonne, Illinois.
155. W. S. Khokley, Department of Electrical Engineering, University of Minnesota, Minneapolis, Minnesota.
156. K. Kimura, Institute of Research Reactor, Kyoto University, Kumatori, Osaka, Japan.
157. O. Klemperer, Imperial College of Science and Technology, University of London, London, England.
158. C. Kunz, Institute fur Angewandte Physik der Universitat, Hamburg, Germany.
159. E. E. LaBate, Bell Telephone Laboratories, Murray Hill, New Jersey.
160. R. E. LaVilla, Crystal Chemistry Section, National Bureau of Standards, Washington, D. C.
161. L. S. Laws, Mathematics Department, Southwestern College, Winfield, Kansas.
162. R. J. Lovell, Physics Department, University of Tennessee, Knoxville, Tennessee.
163. R. C. Lucas, Health Physics Associates, Palo Alto, California.
164. L. Marton, National Bureau of Standards, Washington, D. C..
- 165-
189. M. Y. Nakai, Osaka Lab., Japan Atomic Energy Research Institute, 508 Mii, Neyagawa-City, Osaka, Japan.
190. A. H. Nielsen, Physics Department, University of Tennessee, Knoxville, Tennessee.
191. H. R. Phillip, General Electric Research Laboratory, Schenectady, New York.
192. D. Pines, Department of Physics, University of Illinois, Urbana, Illinois.
193. C. J. Powell, National Bureau of Standards, Washington, D. C.
194. H. L. Pray, Department of Physics, State College of Arkansas, Conway, Arkansas.
195. D. L. Prince, Department of Physics, State College of Arkansas, Conway, Arkansas.
196. J. J. Quinn, R.C.A. Laboratories, Princeton, New Jersey.
197. H. Raether, Institute fur Angewandte Physik der Universitat Hamburg, Hamburg, Germany.
198. A. M. Rauthe, Department of Medical Biophysics, University of Toronto, Toronto, Ontario, Canada.
199. W. O. Roberts, National Corporation for Atmospheric Research, Boulder, Colorado.

200. S. L. Robins, Cornell University, Ithaca, New York.
201. A. K. Roecklein, Montgomery Junior College, Tekoma Park, Maryland.
202. I. Sakurada, Department of Polymer Chemistry, Kyoto, Japan, Kyoto University.
203. P. Schmuser, Institut fur Angewandte Physik der Universitat Hamburg, Hamburg, Germany.
204. T. Sidei, Department of Physics, Kyoto University, Kyoto, Japan.
205. K. Seigbahn, Institute of Physics, University of Uppsala, Uppsala, Sweden.
206. J. Arol Simpson, National Bureau of Standards, Washington, D.C.
207. R. W. Soshea, Health Physics Associates, Palo Alto, California.
208. W. E. Spicer, Stanford Electronics Laboratory, Stanford University, Stanford, California.
209. W. G. Spitzer, Bell Telephone Laboratories, Murray Hill, New Jersey.
210. E. A. Stern, Physics Department, University of Maryland, College Park, Maryland.
211. E. J. Sternglass, Westinghouse Research Laboratories, Pittsburgh, Pennsylvania.
212. R. Stuart, Lawrence Radiation Laboratory, University of California, Livermore, California.
213. J. B. Swan, Department of Physics, University of Western Australia, Nedlands, Western Australia.
214. J. Thomas, Department of Public Health, Yale University, New Haven, Connecticut.
215. R. N. Thomas, Cavendish Laboratory, University of Cambridge, Cambridge, England.
216. K. M. van Vliet, Department of Electrical Engineering, University of Minnesota, Minneapolis, Minnesota.
217. H. Watanabe, Physics Department, Tohoku University, Sendai, Japan.
218. H. J. Watson, Brown Engineering Co., Huntsville, Alabama.
219. F. Wooten, Lawrence Radiation Laboratory, University of California, Livermore, California.
220. A. Ya. Vyatskin, Leningrad Institute of Precision Mechanics and Optics, Leningrad, USSR.
221. J. R. Young, General Electric Research Laboratory, Schenectady, New York.
222. L. Young, University of British Columbia, Vancouver, British Columbia, Canada.
- 223-
237. Division of Technical Information Extension.
- 238-
239. Oak Ridge Associated Universities.